Science
AAAS

Supplementary Materials for

tRNA overexpression rescues peripheral neuropathy caused by mutations in tRNA synthetase

Amila Zuko, Moushami Mallik, Robin Thompson, Emily L. Spaulding, Anne R. Wienand, Marije Been, Abigail L.D. Tadenev, Nick van Bakel, Céline Sijlmans, Leonardo A. Santos, Julia Bussmann, Marica Catinozzi, Sarada Das, Divita Kulshrestha, Robert W. Burgess, Zoya Ignatova, Erik Storkebaum

Correspondence to: e.storkebaum@donders.ru.nl

This PDF file includes:

Materials and Methods

Drosophila genetics

Flies were housed in a temperature-controlled incubator with 12:12 h on/off light cycle at 25°C. *OK371-GAL4* (Bl 26160), *ppk-GAL4* (Bl 32079), *Act5C-GAL4* (Bl 4414), UAS-dS6K^{STDETE} (Bl 6914) and UAS-pAbp (Bl 9148) were obtained from the Bloomington Stock Center (Bloomington, IN), and UAS-dPERK-RNAi (VDRC 110278/KK) and UAS-d4EBP-RNAi (VDRC 35440/GD) were obtained from the Vienna *Drosophila* Resource Center (VDRC). For imaging of Class IV da sensory neurons, *ppk-GAL4* was recombined with *ppk-CD4-tdGFP* (*25*). For the longevity assays, the *tub-GAL4* (Bl 5138) driver was combined with a ubiquitously expressed temperature-sensitive GAL80 under control of the alphaTub84B promoter (Bl 7019).

Generation of tRNA overexpressing *Drosophila* lines

For generation of tRNA$^{Gly\text{-}GCC}$ BAC transgenic *Drosophila* lines, the bacterial artificial chromosome (BAC) CH322-72N10 (*26*) containing 5 tRNA$^{Gly\text{-}GCC}$ genes was used for embryo injection following standard procedures, using VK22 and VK20 genomic landing sites for transgene insertion on the second and third chromosome, respectively.

For generation of tRNA$^{Gly\text{-}GCC}$ 'scramble' transgenic *Drosophila* lines, genomic DNA extracted from w^{1118} flies was used as a template for PCR amplification of tRNA$^{Gly\text{-}GCC}$ genes (tRNA:Gly-GCC-1-1 (2x), tRNA:Gly-GCC-1-2 (2x), tRNA:Gly-GCC-1-3, tRNA:Gly-GCC-1-8 (2x), tRNA:Gly-GCC-1-9, tRNA:Gly-GCC-1-11 and tRNA:Gly-GCC-1-13) along with at least 700 nt upstream and 300 nt downstream sequences to ensure inclusion of regulatory sequences. Each PCR fragment was separately cloned into the pJet1.2 plasmid (CloneJET PCR Cloning Kit, Thermo Scientific) and sequence verified. Gibson assembly was used to generate 3 separate plasmids, each with a combination of 3 or 4 tRNA Gly-GCC genes in a pENTR plasmid backbone. Via restriction cloning the 3 plasmids were combined to a single 10x tRNA$^{Gly\text{-}GCC}$ pENTR plasmid. The 10x tRNA$^{Gly\text{-}GCC}$ fragment was subsequently cloned into the pBID plasmid backbone (*27*) using NotI and XhoI. The resulting construct (Fig. 1A) was used for embryo injection following standard procedures, using VK22 and VK27 genomic landing sites for transgene insertion on the second and third chromosome, respectively.

For generation of tRNA$^{Gly\text{-}UCC}$ transgenic *Drosophila* lines, Gibson assembly was used for generation of a construct that contains three copies of a genomic fragment which contains two tRNA$^{Gly\text{-}UCC}$ genes (tRNA:Gly-TCC-1-3 and tRNA:Gly-TCC-1-4) and at least 700 nt upstream and 300 nt downstream sequences (Fig. 1A). BAC clone CH322-79F21 was used as a template for PCR amplification of the genomic fragment, and pEntr (Thermo Scientific) was used as a template for PCR amplification of a plasmid backbone. The resulting construct was sequence-verified and cloned into pBID (*27*) using KpnI and XbaI, and used for embryo injection following standard procedures, using VK22 and VK20 genomic landing sites for transgene insertion on the second and third chromosome, respectively.

For both tRNA$^{Gly\text{-}GCC}$ 'scramble' and tRNA$^{Gly\text{-}UCC}$ transgenic constructs, Phusion high-fidelity DNA polymerase (New England Biolabs) was used for PCR, in combination with the primer pairs listed in Table S5. The NEBuilder online tool (New England Biolabs) was used to design the primers.

Meiotic recombination was used to generate recombinant chromosomes that contain both a UAS-GlyRS and a tRNA^{Gly} transgene on either the second or the third chromosome. Subsequently, stocks were generated which contain UAS-GlyRS, tRNA^{Gly} transgenes on both

the second and third chromosome. These stocks were crossed to the relevant GAL4 driver to obtain the experimental genotypes. For controls overexpressing the $tRNA^{Gly}$ transgenes alone, stocks were generated which contain $tRNA^{Gly}$ transgenes on both the second and third chromosome.

Analysis of protein synthesis by *in vivo* FUNCAT

For FUNCAT analysis of protein synthesis (*9, 13, 28*), 4 h egg collections were performed and animals were raised on Jazz-Mix *Drosophila* medium (Fisher Scientific) at 25 °C. 72 h AEL, larvae were transferred to 4 mM azidonorleucine (ANL, Iris Biotech, HAA1625.0025, Cas#: 159610-92-1net)-containing medium for 48 h. Larval central nervous system (CNS) was dissected in ice-cold HL3 solution and fixed in 4% paraformaldehyde (PFA) for 30 min at RT. After fixation, the CNSs were washed 3 x 10 min with PBST (1x PBS pH 7.2 containing 0.2% Triton X-100) and 3 x 10 min with PBS pH 7.8. Metabolically labeled proteins were tagged by 'click chemistry' (Copper-Catalyzed (3+2)-Azide-Alkyne-Cycloaddition Chemistry (CuAAC)) using the fluorescent tag TAMRA. The FUNCAT reaction mix was assembled in a defined sequence of steps. Triazole ligand (1:1000), TAMRA-alkyne tag (1:5000; Sigma Aldrich, 900932), TCEP solution (1:1000) and CuSO4 solution (1:1000) were added to PBS pH 7.8. After each addition the solution was mixed thoroughly for 10 sec and at the end for 30 sec using a high-speed vortex. Larval brains were incubated with 200 µl of FUNCAT reaction mix overnight at 4 °C on a rotating platform. The next day, the brains were washed 3 times with PBS-Tween and 3 times with PBST for 10 min. Finally, larval CNSs were mounted in VectaShield mounting medium (Biozol, VEC-H-1000-CE) and stored at 4 °C until imaging using a Leica SP8 laser scanning confocal microscope. For image acquisition, identical confocal settings were used for all samples of a given experiment. Fluorescence intensities were quantified using ImageJ/FIJI software (National Institutes of Health). Mean intensity of all cells within one motor neuron cluster from each ventral nerve cord were used as single data points for statistical analysis.

Adult offspring frequency

To evaluate adult offspring frequencies, virgin females heterozygous for a GAL4 driver over a balancer chromosome were crossed to males homozygous for a UAS-transgene alone or a UAS-transgene combined with $10xtRNA^{Gly\text{-}GCC}$ or $12xtRNA^{Gly\text{-}UCC}$ transgenes, and maintained at 25°C. F1 progeny with and without balancer were counted for 9 days after eclosion of the first F1 flies, and the percentage of non-balancer flies was calculated and plotted as percentage of the driver-only control.

Analysis of larval muscle innervation

To analyze innervation of larval muscle 24 and synapse length on muscle 8, third instar larvae were dissected in HL3 buffer and fixed in Bouin's for 3 min. After permeabilization and blocking (10% goat serum), immunostaining was performed with anti-Discs large 1 (anti-dlg1; mouse monoclonal 4F3; DSHB, 1/200). Images were taken of muscle 8 in abdominal segment 5 using a Leica SP8 laser scanning confocal microscope with 20x Plan-Apochromat objective (0.8 NA). Maximum intensity projections of z-stacks comprising the entire NMJ were used to measure the synapse length. The innervation status of muscle 24 was evaluated by scoring the presence ('innervated') or absence ('denervated') of dlg1 staining.

Automated negative geotaxis assay to analyze motor performance

To assay motor performance, virgin female flies were collected and divided into groups of 10 individuals. Until measurement, flies were maintained at 25°C with a 12-h light/dark cycle on standard *Drosophila* medium. 7-day-old flies were evaluated in a rapid iterative negative geotaxis assay (RING-assay), which had been previously established in our lab (*9*). The assay is based on the innate escape response of flies to climb up the wall of a vial after being tapped down to its bottom. Flies were transferred into test tubes without anesthesia and three iterative measurements of at least 8 groups of 10 flies per genotype were video recorded with a Nikon D3100 DSLR camera. The resulting movies were converted into 8-bit grayscale TIF image sequences with 10 frames/s. Subsequently, image sequences were analyzed using an MTrack3 plug-in that automatically imports images in ImageJ, subtracts backgrounds, and filters and binarizes images to allow tracking of flies. Average climbing speed (mm/s) of all tracked flies was determined, averaged per test tube, and compared between genotypes.

Analysis of sensory neuron dendritic morphology

Class IV da sensory neuron morphology imaging was performed on living third instar larvae. Microscopy slides were prepared with two coverslips glued on as spacers with conventional superglue. Larvae were thoroughly washed in tap water and single chilled larvae were immobilized under a coverslip, which itself was glued onto the spacing coverslips to provide equal spacing and pressure on the larvae. Only dorsal class IV da neurons of larval segment A1 were imaged using a Leica SP8 laser scanning confocal microscope. For quantification, maximum intensity projections were processed with Adobe Photoshop, rotated and digitally placed under a transparent grid containing a crosshair. The crosshair was used to fit the grid onto the cell body of the class IV da neuron in order to divide the dendritic tile into four quadrants. The posteromedial quadrant of the imaged da neuron was chosen for quantification of dendritic coverage, as least imaging artifacts and interference of denticle bands were encountered in that area. For quantification within the posteromedial quadrant, a sector of 200 µm to the medial and 280 µm to the posterior was defined, equaling 56,000 μm^2 divided into 560 squares of 8 x 8 pixels each. Presence versus absence of a piece of dendrite in the defined boxes was scored and calculated as measure of relative dendritic coverage.

Life span analysis

To evaluate life span, the TARGET system was used to conditionally express UAS-GlyRS transgenes from the adult stage onwards, with or without the $10xtRNA^{Gly\text{-}GCC}$ or $12xtRNA^{Gly\text{-}UCC}$ transgenes. The *tub-GAL4* driver was combined with a ubiquitously expressed temperature-sensitive GAL80 (*tub-GAL80^{ts}*). Fly crosses were cultured at 18°C (permissive temperature) and adult progeny carrying the *tub-GAL4, tub-GAL80^{ts}* and UAS-GlyRS transgenes with or without the $10xtRNA^{Gly\text{-}GCC}$ or $12xtRNA^{Gly\text{-}UCC}$ constructs was shifted to 29°C to induce transgene expression. Females were collected within 4-8 h of eclosion and grouped into batches of 10 flies per food vial. The number of dead flies was counted every day and flies were transferred to fresh food vials every 2–3 days. At least 70 flies per genotype were used.

Western blotting

For Western blots of *Drosophila* tissues, protein extracts were made by homogenizing third instar larval CNS in extraction buffer (50 mM Tris/HCl pH 7.4, 150 mM KCl, 0.25 M sucrose, 5 mM MgCl2, and 0.5% Triton X-100 containing 1 U complete mini protease inhibitor cocktail

(Roche)). Samples separated on 10% SDS-PAGE were electrotransferred onto polyvinylidene difluoride (PVDF) membranes (EMD Millipore) for 45 min at 15 V. Blotted membranes were incubated overnight at 4°C with primary antibodies against hGlyRS (rabbit polyclonal; 1:200; Proteintech, 15831-AP), and β-tubulin (mouse monoclonal E7; 1:700; DSHB). Immunoreactive proteins were visualized after incubation with anti-rabbit and anti-mouse IgG coupled to horseradish peroxidase (W4011; W4021; 1:2,500; Promega) for 1 h at RT. Blots were developed with enhanced chemiluminescence (GE Healthcare), and x-ray film images of chemiluminescence were developed and scanned. Densitometric quantification of images was performed with ImageJ/FIJI (National Institutes of Health).

For Western blots of mouse tissues, protein was extracted from tibialis anterior muscle and spinal cord tissue by use of lysis buffer (20mM Tris, 0.1% SDS, 150mM NaCl, 1mM EDTA, 5% Glycerol, 1% Triton X-100, 1x Protease inhibitor, 1mM PMSF, 1mM NaF, 2mM Na_3VO_4, 20mM $Na_4P_2O_7$, pH 7.4). Biological and technical replica samples were separated on 10% SDS-PAGE gels and transferred to PVDF membranes (EMD Millipore). The blotted membranes were blocked with 5% Milk in TBS-T and incubated with rabbit anti-GlyRS (ab42905, Abcam, 1:1000), mouse anti-tubulin beta (E7, DSHB, 1:1000) and mouse anti-actin (JLA20, DSHB, 1:1000) primary antibodies. Subsequently, the membranes were washed with TBS-T and incubated with secondary IgG coupled to HRP. The membranes were washed with TBS-T and incubated with ECL. Images were captured with the ImageQuant LAS-4000. ImageJ/FIJI (National Institutes of Health) was used for densitometric quantification of band intensities.

Northern blotting

To evaluate tRNA levels in mouse or *Drosophila* tissues, total RNA was extracted using Trizol reagent (Life Technologies). For tRNA northern analysis, total RNA was loaded on denaturing 15% polyacrylamide gels and blotted onto Hybond-N+ membranes (GE Healthcare Life Sciences). The membrane was hybridized with 5' end-labeled DNA oligo probes (Table S6) at 42 ºC in a hybridization buffer containing 6x SSC, 0.01M sodium phosphate pH 6.8, 1mM EDTA, 0.25% SDS and 100 µg/ml salmon sperm DNA. Blots were washed with 1x SSC, 0.1% SDS at 42 ºC (2 times 15 min). Phosphor screens were exposed to the blots for at least 2 h and imaged on a Typhoon FLA7000 scanner (GE Healthcare). Band intensity was determined using ImageJ/FIJI (National Institutes of Health).

Mouse work

Mouse experiments performed at the Radboud University (Nijmegen, Netherlands) were approved by the national Dutch ethics committee 'Centrale Commissie Dierproeven' (AVD1030020184826/2017-0067). For mouse experiments performed at The Jackson Laboratory (Bar Harbor, ME, USA), all mouse husbandry and experimental procedures were conducted according to the NIH *Guide for Care and Use of Laboratory Animals* and were reviewed and approved by The Animal Care and Use Committee of The Jackson Laboratory, Bar Harbor, ME, under Animal Use Summary 1026. The terminal procedures were performed at 8, 12 and 52 weeks of age. All mice were maintained in a vivarium on a 12:12 light/dark cycle and were provided food and water ad libitum.

The $Gars^{C201R/+}$ mice (C3H.C-GarsC201R/H) (*15*) carry an ENU-induced dominant point mutation that causes a cysteine to arginine substitution at residue 201 of the GlyRS protein. In $Gars^{\Delta ETAQ/+}$ mice (*16*), a 12 nt deletion was introduced in the endogenous mouse *Gars* gene to mimic a patient mutation which results in the in-frame deletion of 4 amino acids in GlyRS (245-

248_delETAQ). The nmf205 mutant mouse (C57BL/6J-Gtpbp2<nmf205>/J; Stock#004823) (*20*) was identified in an ENU-mutagenesis screen of C57BL/6J (B6J) mice for neurological phenotypes at The Jackson Laboratory. The nmf205 mutation is a point mutation in the consensus splice donor site of intron 6 of *Gtpbp2*, which results in mRNAs with premature stop codons and no expression of GTPBP2. Loss of GTPBP2 in B6J mice results in cerebellar ataxia by 5-6 weeks of age and death between 8-9 weeks of age. The *n-Tr20* congenic mouse (B6J.B6N-n-Trtct5<C57BL/6N/SlacCx; private colony) expresses C57BL/6N (wild-type) *n-Tr20*, one of 5 isodecoders of the $tRNA^{Arg\text{-}UCU}$ family (*20*). When $Gtpbp2^{-/-}$ mice express at least one copy of wild-type *n-Tr20*, neurodegeneration is attenuated. Heterozygous stock colonies of *Gtpbp2*, $Gars^{C201R}$, and *n-Tr20* mice were maintained. $Gtpbp2^{+/-}$ mice were separately crossed with $Gars^{C201R/+}$ and $n\text{-}Tr20^{+/-}$ mice to create $Gtpbp2^{+/-}$; $Gars^{C201R/+}$ and $Gtpbp2^{+/-}$; $n\text{-}Tr20^{+/-}$ lines. These lines were then crossed to create the genotypes needed for our study. In mouse experiments performed at the Radboud University, all mouse lines were in the C57Bl/6J background. Primers used for mouse genotyping are listed in Table S7.

Generation of $tRNA^{Gly\text{-}GCC}$ transgenic mouse lines

Mouse genomic DNA was extracted from mouse tail biopsies using the Nucleospin Tissue Kit (Macherey-Nagel). A 1798 nt genomic DNA fragment containing the chr8.trna383-Gly-GCC and chr8.trna384-Gly-GCC genes was PCR amplified using Phusion High-Fidelity DNA polymerase (New England Biolabs) and the primers listed in Table S5. The resulting PCR fragment was gel purified and cloned (Zero Blunt TOPO PCR Cloning Kit, Thermofisher Scientific). Positive clones were amplified and purified, and verified by restriction digest (EcoRV and SpeI) and sequencing using M13 forward and reverse primers, as well as the primers listed in Table S5.

The linear DNA fragment used for zygote injection was excised from the TOPO backbone by restriction digestion with EcoRV and SpeI, gel purified, and microinjected into C57BL/6 zygotes by Taconic Biosciences. For genotyping, gDNA was extracted from ear punch biopsies and analyzed by PCR using the primers listed in Table S7. For initial characterization, primer pairs to detect the 5' fusion between the remaining TOPO vector fragment and the genomic transgene (primers tRNA-gly-GCC-5'_FW and tRNA-gly-GCC-5'_REV, yielding a 396bp fragment), the 3' fusion between the remaining TOPO vector fragment and the genomic transgene (primers tRNA-gly-GCC-3'_FW and tRNA-gly-GCC-3'_REV, yielding a 336bp fragment), and an internal control fragment (primers CD79b_FW and CD79b_REV to amplify a 585bp fragment of the wild type CD79b allele on Chromosome 11 to confirm the presence of genomic DNA) were used.

Copy number and TLA analysis of $tRNA^{Gly\text{-}GCC}$ transgenic mouse lines

The copy number of the genomic fragment that was used for generation of $tRNA^{Gly\text{-}GCC}$ transgenic mouse lines was estimated by quantitative real-time PCR (TaqMan Assay), using the primers and probe listed in Table S8. As a reference TaqMan Assay, primers and probe for the mouse Tert gene were used (Applied Biosystems #4458368). The obtained relative values were normalized to an average copy number of 2 for the wild type control mice (as the mouse genome contains 2 allelic copies of this genomic fragment).

Transgenic locus amplification (TLA) was performed by Cergentis, using viable frozen bone marrow cells derived from $tRNA^{Gly\text{-}high}$ mice, according to a previously described protocol (*29*). Two independent transgene-specific primer sets were used (Table S8). The NGS reads were

aligned to the transgene sequence and host genome. The mouse mm10 genome was used as host reference genome sequence. High coverage was observed across the transgene sequence and no sequence variants were detected in the transgene. Four transgene-transgene breakpoints were found, indicating that transgene sequences are concatemerized.

Quantitative real-time PCR (qPCR)

Total RNA was extracted from spinal cord using Trizol reagent (Life Technologies). Following DNase treatment, the SensiFAST cDNA synthesis kit (BioLine) was used for reverse transcription to cDNA, using 500ng RNA as starting material. Resulting cDNA samples were used as templates for real-time PCR assays performed on a BioRad CFX system using the SensiFAST SYBR No-ROX Kit (BioLine). Primers used for quantification of ATF4 target genes are listed in Table S8. Beta-actin mRNA was used as housekeeping gene for normalization. Data were analyzed using the ΔΔCt calculation method. Experiments included no-reverse transcriptase and no-template controls for each primer pair.

Analysis of mouse motor performance

Inverted grid test. As previously described (*30*), mice were placed on a grid which then was inverted and held approximately 30 cm above a mouse cage with bedding. The latency to fall (s) was timed and recorded, up to a maximum of 60s. The test was performed 2 to 3 times per session and a rest period of at least 30 seconds was given between individual trials. The average of the trials is reported for each testing day.

4-paw grip strength. Mice were placed on a grid connected to a dynamometer (Bioseb) and gently pulled off by their tail. The maximal peak force applied by the mouse on the grid was recorded. The measurement was repeated three times, and the average value per mouse and per time point was used for statistical analysis.

Electromyography

EMG was performed as previously described (*30*) to measure nerve conduction velocity of the sciatic nerve and compound muscle action potential (CMAP) in the gastrocnemius muscle. Mice were anesthetized by use of ketamine/xylazine (100 mg/kg; 5 mg/kg) or isoflurane (2%). Electrical activity was recorded in gastrocnemius muscle of both legs by use of monopolar needle electrodes. CMAP was triggered by supramaximal square pulses (0.05 ms duration) to the sciatic nerve at the sciatic notch level. The average amplitude of muscle responses from both sides was calculated and used as a data point to report the CMAP. The time between electrical stimulation of the sciatic nerve and the muscle response was measured and reported as the latency time. NCV was calculated as [conduction distance/(proximal latency-distal latency)] (*31*).

Histological analysis of mouse tissues

Muscle weight analysis. At 12 or 52 weeks of age, gastrocnemius muscles were dissected and their weight was immediately determined.

NMJ immunohistochemistry and analysis of innervation status. The plantaris muscle was dissected and fixed in 2% PFA (overnight at 4 °C). The tissue was washed with PBS and blocked with PBS containing 5% normal goat serum and 0.5% Triton-X 100 for 1 h followed by a rough teasing and flattening the muscle by pressing between two glass slides for 30 min in blocking solution. To visualize the nerves, the flattened muscle was incubated with mouse anti-synaptic

vesicle glycoprotein 2A (SV2, DSHB, 1:20) and mouse anti-neurofilament (2H3, DSHB, 1:100) in blocking solution (overnight at 4 °C). The tissue was washed with PBS containing 0.5% Triton-X 100 and incubated with goat anti-mouse 405 (A31553, Invitrogen, 1:300) and TRITC-conjugated BTX (T0195, Sigma, 1:500; to visualize postsynaptic acetylcholine receptors) overnight at 4 °C in blocking solution. The muscle tissue was washed with PBS containing 0.5% Triton-X 100 and mounted with Fluorsave (Merck Millipore). Immunoreactive structures were imaged at 40x (Oil) magnification on a Leica Sp8 Liachroic confocal microscope. 50 NMJs per sample (n = 5 per group) were randomly captured. ImageJ/FIJI (National Institutes of Health) was used to quantify the innervation status, which was evaluated based on the alignment of juxtaposed pre- and postsynapses. NMJs with >80% of overlap were classified as innervated, <80% as partially innervated, and <1% as denervated.

Phosphorylated eIF2α immunohistochemistry and analysis of staining intensity. Mice were perfused with PBS and 1% paraformaldehyde (PFA). The spinal cords were dissected, and the lumbar section was post-fixed in 1% PFA (overnight at 4 °C) and cryoprotected in 30% sucrose (overnight at 4 °C). The lumbar spinal cords were embedded in optimum cutting temperature (OCT; VWR), frozen in cold 2-methyl butane, and kept at -80 °C until sectioning. 20µm cryosections were made, dried for 30 minutes and permeabilized with 0.5% Triton-X 100 in TBS for 1 h. The sections were blocked with TBS containing 2% normal donkey serum and 0.5% Triton-X 100 for 1 h followed by incubation with rabbit anti-peIF2*α* antibody (9721S, Cell Signaling, 1:100 diluted in blocking buffer) for 72 h at 4 °C. The sections were washed in TBS containing 0.5% Triton-X 100 and incubated with donkey anti-rabbit 488 (A32790, Thermofisher, 1:500) for 2 h at room temperature in blocking solution. The sections were washed in TBS containing 0.5% Triton-X 100, incubated in DAPI before they were washed again in TBS and embedded in Hardset Vectashield (H1400, Vectorlabs). The stained sections were imaged at 20x magnification on a Leica Sp8 Liachroic confocal microscope. Bilateral ventral horns of the spinal cords were captured per animal (n=4-5 per group). ImageJ/FIJI (National Institutes of Health) was used to quantify the mean intensity per cell area (μm^2) of peIF2*α* positive-cells in the ventral horn. The average mean intensity of all peIF2*α* positive-cells per animal was calculated, in order to obtain one data point per animal for statistical analysis.

Axon histology. The femoral nerves, which include both a motor and sensory branch (*32*), were dissected free and fixed by immersion in 2% PFA, 2% glutaraldehyde in 0.1M cacodylate buffer overnight at 4°C. Nerves were then placed in PBS and kept at 4°C until sectioning. Nerves were plastic embedded, sectioned at 0.5 µm thickness, and stained with Toluidine Blue. Images were collected at 40X magnification on a Nikon Eclipse 600 microscope with DIC-Nomarski optics. Images were analyzed for axon number using an automated method in ImageJ/FIJI (National Institutes of Health) that was manually confirmed by visual inspection of images for mis-identified axons. The diameter of all axons per motor branch was measured in ImageJ/FIJI (National Institutes of Health) with the Measure & Label Plug-in.

Fluorescence in situ hybridization. The *in situ* hybridization probes used to detect mRNA encoding *Chat* (408731-C2), *Gdf15* (318521), *Adm2* (497111), *B4galnt2* (529871), *Fgf21* (Cat# 460931-C3), *Cdsn* (Cat# 475831-C3) and *Gtpbp2* (527461) were designed by Advanced Cell Diagnostics (Newark, CA, USA). Further products (probe diluent, protease, fluorescent multiplex detection, wash buffer, HybEZ Hybridization System) were also purchased from Advanced Cell Diagnostics. Lumbar spinal cords were dissected and directly embedded in OCT compound (Sakura) following a 'cryo-no-fix' procedure. 12 µm transverse sections were made using a cryostat, mounted onto Superfrost Plus Slides, and stored at -20°C until use. Sections of

all genotypes were mounted on the same slide within a .75 by .75 inch area for consistent further processing. Labeling of the lumbar spinal cord sections for the different mRNAs was performed in separate experiments with different probe combinations. Solutions were prepared in DEPC-treated water (0.1% diethyl pyrocarbonate). Spinal cord sections were taken from -80 °C and directly processed by incubation in cold 4% PFA (5 min). The sections were dehydrated by incubating in solutions with increasing EtOH concentrations (once 50%, once 70%, twice 100%) and completely dried at room temperature. The sections were encircled with a hydrophobic barrier pen and treated with Protease IV for 30 minutes at room temperature, followed by washing with PBS and incubation with probe solution for 2 h at 40 °C in the HybEZ Hybridization System. Subsequently, the sections were incubated with fluorescent multiplex detection reagent 1 (30 minutes), 2 (15 minutes), 3 (30 minutes) and 4 (Alt A-FL; 15 minutes) at 40 °C in the HybEZ Hybridization System to conjugate the fluorophores to the target mRNA. Before and after incubation with the reagent, the sections were washed with wash buffer. After washing the sections with PBS, the sections were incubated in DAPI and embedded in ProLong Glass Antifade Mountant (ThermoFisher P36980). The sections were imaged at 20x magnification on a Leica Sp8 Liachroic confocal microscope. The positive signal area of the different probes within Chat-positive motor neurons in the ventral horn of the spinal cord were measured. The positive signal area size per motor neuron was averaged over all motor neurons per animal, in order to obtain one value per animal for statistical analysis.

For fluorescent in situ hybridization experiments on spinal cord of $Gars^{C201R}$ x $Gtpbp2^{KO}$ mice, single plane images were taken on a Zeiss 2 Axioimager at 20x magnification and tiled images were stitched using Adobe Photoshop. The percent of motor neurons positive for other probes was obtained as follows. All images for these studies were taken with identical microscope settings. Isolated Chat signal was used to delineate each motor neuron in ImageJ. The delineated areas were then overlaid on isolated signal for the other in situ hybridization probes, and each area was categorized as positive or negative. One spinal cord section was analyzed per mouse. The percent of positive motor neurons was calculated for each mouse and used for statistical analysis. This analysis was performed blind to genotype.

Expression and purification of recombinant GlyRS proteins

All GlyRS variants were cloned into pET28 modified with two expression tags, i.e. 6xHis and SUMO tag, and expressed in the *E. coli* Rosetta strain. Cultures were grown until the exponential phase (OD_{600} = 0.7-0.8) and induced with 0.7mM IPTG for 16h at 22°C. GlyRS variants were bound to *HisPur Ni-NTA resin* (Thermo) by incubating for 30 minutes at 4 °C, washed multiple times with 20 mM Tris-HCl pH 8.0, 500 mM NaCl, and 10 mM imidazole, followed by twice washing with 20 mM Tris-HCl pH 8.0, 500 mM NaCl, and 20 mM imidazole. The GlyRS variants were eluted from the resin by cleaving the SUMO tag by incubating the resin with 0.5 mg/mL of ULP overnight at 4ºC. The collected supernatant was concentrated using *Vivaspin 20* spin columns, followed by fractionation of dimer and monomer forms via size-exclusion chromatography on *Superdex 200.*

Determination of K_{on} and K_{off} values

K_{on} values for the cognate $tRNA^{Gly\text{-}GCC}$ or $tRNA^{Gly\text{-}UCC}$ were determined by monitoring the quenching of intrinsic tryptophan residues. In a 96-well plate format using multiple replicates, 750 nM of each GlyRS variant was incubated with different tRNA concentrations, ranging from 0-1µM, in 25 mM sodium acetate buffer pH 6.0 containing 10 mM $MgCl_2$, 5 mM DTT, in final

volume of 50µL and Trp emission was recorded at 350nm (excitation 280 nm) at 37 °C on a *TECAN Spark* plate-reader. $tRNA^{Gly\text{-}GCC}$ and $tRNA^{Gly\text{-}UCC}$ were generated via *in vitro* T7 transcription and purified via 10% polyacrylamide gel electrophoresis. Binding curves were fitted to exponential decay functions and quantified with *OriginPro*.

For determination of K_{off} values, between 0.1-1µM $tRNA^{Gly}$ was added to 750 nM of each GlyRS variant in 25 mM sodium acetate buffer pH 6.0 containing 10 mM $MgCl_2$, 5 mM DTT and incubated for 10 min at 37 °C (final volume of 50 µL). To each reaction, glycine and ATP, each 1 mM, were added to the wells. Fluorescence spectra (emission at 350 nm and excitation at 280 nm) were recorded over 5 min, step 1 s. Spectra were fitted in *OriginPro* to an exponential function. For each variant more than 50 traces, in biological replicates setting, were recorded. For the CMT-mutant GlyRS variants that strongly bind $tRNAs^{Gly}$, albeit rarely, we detected some events of tRNA release. Those curves were fitted and discrete K_{off} values reported along with the fraction of the cases for which we registered them (Fig. 3B and Table S2).

The stability of $tRNA^{Gly}$:GlyRS complexes depends on both K_{on} and K_{off}, i.e. K_D value ($K_D=K_{on}/K_{off}$) which largely differs among the variants. Along with K_D, mean life and the half-life of a protein:ligand complex (i.e. $1/K_{off}$ and $\ln 2/K_{off}$, respectively) are quantitative predictors on its stability (*33*). Together, K_D and $1/K_{off}$ of the $tRNA^{Gly}$-GlyRS complexes quantitatively recapitulate the tRNA sequestration effect for all CMT-mutant GlyRS proteins.

Modeling the level of $tRNA^{Gly}$ overexpression needed for rescue

The translation rate of a single codon depends on (i) tRNA aminoacylation by the cognate aaRS; (ii) ternary complex formation with elongation factor eEF1A and its free diffusion to ribosomes; (iii) tRNA recycling mediated by eEF-1B/C (*34*). Using the mathematical formalism for describing the translation process (*34*), the mass balance is described by:

$$\frac{d(f[\mathrm{tRNA}])}{dt} = \frac{k_{cat}(1-f)[\mathrm{tRNA}]}{K_m+(1-f)[\mathrm{tRNA}]}[\mathrm{aaRS}] + k_t f[\mathrm{tRNA}]m \qquad (1)$$

where k_{cat} and K_m are the kinetic parameter of the aaRS for tRNA aminoacylation, [tRNA] and [aaRS] are the total concentration of a tRNA species and the cognate aaRS, respectively, f is the fraction of charged tRNA and k_t is the rate constant of translation of a codon which is translated by a fraction of the ribosomes m. The left term in Eq. 1 depends on the aaRS enzymatic properties and the right term, $r_t = k_t f[\mathrm{tRNA}]m$, describes the rate of translation of a codon. Taking translation of Gly codons as example, under non-limiting Gly amino acid supply which is the case in balanced fed mammalian cells, k_{cat} = 0.2-0.7 s^{-1} and K_m = 0.28-1.37.10^{-6} M for $tRNA^{Gly}$ (the parameters were taken from the enzyme database BRENDA). Since the precise ribosome and total tRNA concentration for the specific tissue is unknown, we used averaged values for a eukaryotic cell, i.e. 30-100 µM total tRNA concentration and 1-10 Mio ribosomes/cell (https://bionumbers.hms.harvard.edu). Using the quantitative sets of HeLa and HEK293T tRNAs (*35, 36*), in a total tRNA concentration of 30-100 µM, the concentration of $tRNA^{Gly}$ isoacceptors is 0.5-1.7 µM. The maximal concentration of the ribosomes which could simultaneously request all four Gly codons can be estimated from the cumulative Gly codon usage and is calculated to be 8.3x10^{-7} M. At steady state f=0.8, i.e. 80% of the tRNA is charged (*37*). The concentration of GlyRS is estimated from its K_m value to be 0.5-2.4.10^{-6} M. Numerically solving Eq. (1) using k_t for wild-type GlyRS, taking the mean values for all parameters, we obtained that the rate of translation (r_t) and k_t for Gly codons are r_t=0.16x10^{-6}

mol.l^{-1}.s^{-1} and k_t=0.22x10^{-6} s^{-1}, respectively. The average waiting time for the ribosome for a cognate ternary complex at a codon is determined from:

$$\tau = \frac{1}{k_t f [\text{tRNA}]} \quad (2)$$

Solving Eq (2) for Gly codon results in 4.5 Gly codons/s. This result is consistent with the experimentally measured translation rate in eukaryotic cells (1-7 codons/sec).
Since GlyRS mutations are heterozygous and assuming equal expression from both alleles, the average GlyRS concentration will be 0.8 µM wild-type GlyRS and 0.8 µM mutated GlyRS. The markedly slower tRNA^{Gly} release for L129P, C157R, G240R, and G526R GlyRS (i.e. $K_{off} = \infty$) from the dimers and monomers suggests at steady-state a full saturation of the mutant GlyRS. As a result, the mutant GlyRS will sequester 0.8 µM tRNA^{Gly}. To restore the function of the wild-type GlyRS counterpart, i.e. to reach the wild-type GlyRS translation rate of r_t=0.16x10^{-6} mol.l^{-1}.s^{-1}, using Eq. 1 we model that the concentration of tRNA should be increased up to 1.9 µM, i.e. a raise of the total tRNA^{Gly} concentration by 1.7-fold is necessary. For the E279D and E71G, considering the dimer:monomer ratio and that the monomer only sequesters the tRNA, an increase of tRNA by 1.3-fold and 1.1-fold respectively would rescue these mutations.

In vivo quantification of tRNA^{Gly} bound to GlyRS

Brains from *Gars*$^{C201R/+}$ mice and littermate controls were dissected and snap frozen. Frozen brains were grinded, subjected to UV-crosslinking at 254 nm, 400mJ/cm^2 (UVP-TL-2000 Translinker) after which lysis buffer (20mM Tris-HCl pH 7.4, 15mM NaCl, 1% NP-40, 0.1% Triton-100,0.5%SDC, 2mM DTT, protease inhibitor) was added. Protein-G-Dynabeads (Invitrogen) were coupled with GlyRS antibody mixture (rabbit polyclonal; 1:400; Abcam, ab42905 and rabbit polyclonal; 1:200; Proteintech, 15831-AP) and incubated with the lysed tissue overnight at 4°C. Beads were precipitated by centrifugation and washed with buffer (20mM Tris-HCl pH 7.4, 100mM NaCl, 1% NP-40, 0.1% Triton-100,0.5%SDC,2mM DTT). The tRNA bound to GlyRS (co-immunoprecipitated with the GlyRS-antibodies-coated Dynabeads) was extracted with phenol:chloroform (Sigma) and subjected first to tRNA identification, followed by quantification. By this extraction the tRNA is completely deacylated.
The identity of tRNAs bound to the immunoprecipitated GlyRS was determined by Northern blot using Atto565-labeled stoichiometric mixture of degenerated DNA oligonucleotides specifically recognizing the three tRNA^{Gly} isoacceptors with the following sequences: 5'-CCCGGGTCAACTGCTTGGAAGGCAGCTAT-3', and 5'-GYCTCCCGCGTGGSAGGCGAG-3'.
For quantification of the GlyRS-bound tRNA, we used Cy3-labeled fluorescent stem-loop RNA/DNA oligonucleotide that ligates to the unpaired 3'-NCCA end of the tRNAs^{Gly} (5'-pCGCACUGCdTdTXdTdTdGdCdAdGdTdGdCdGdTdGdGdN-3'). The total tRNA extracted from the immunoprecipitated GlyRS from *Gars*$^{C201R/+}$ and WT mice, in five biological replicates (one wild type and one *Gars*$^{C201R/+}$ brain per replicate), was ligated with the fluorescent oligonucleotide as described (*36*), loaded on 10% denaturing polyacrylamide gel and the fluorescent signals were quantified using ImageJ.
GlyRS bound to the GlyRS-antibodies-coated Dynabeads was quantified by the capillary electrophoresis immunoblotting system (Jess, ProteinSimple) using GlyRS antibody (rabbit polyclonal; 1:200; Proteintech, 15831-AP) as described previously (*38*). A standard curve was obtained using purified wild type GlyRS.

Ribosome profiling

Spinal cord of three *Gars*$^{C201R/+}$ and three WT littermate control mice were flash frozen and immediately lysed by grinding in 10mM Tris-HCL pH 7.4, 5mM $MgCl_2$, 100mM KCL, 1% NP-40, 2% sodium deoxycholate. The lysates from three animals per genotype were pooled. Cycloheximide (100 µg/ml) was added to the sucrose gradient fractions when collecting polysomes to prevent ribosomal dissociation during RNase I digestion. The lysates from three animals per genotype were pooled. Isolation of mRNA-bound ribosome complexes, RNase I digestion-derived ribosome-protected fragments (RPFs) and the cDNA libraries from RPFs were prepared using a protocol for miRNA with direct ligation of the adapters (*39*). Sequenced reads were trimmed using *fastx-toolkit* (0.0.13.2; quality threshold: 20), adapters were cut using *cutadapt* (1.8.3; minimal overlap: 1 nt), and processed reads were uniquely mapped to the mouse genome (GRCm38) using STAR (2.5.4b) (*40*), allowing a maximum of one mismatch, with parameter settings: --outFilterMismatchNmax 1 --outFilterType BySJout –outFilterMultimapNmax. Uniquely mapped reads were normalized to reads per kilobase per million mapped reads (RPKM).

To calibrate the RPFs, i.e. to determine position of the A-site codon within each RPF, the RPFs were binned into groups of equal read length, and each group was aligned via P-site positioning over the start codon as described (*20, 41*), using the calibration tool (https://github.com/AlexanderBartholomaeus/MiMB_ribosome_profiling) (*42*). Briefly, bins were separately plotted to cover the initiation and early elongation (app. 300 codons). Ribosomes spanning the start codon accommodate AUG at their P-site, causing a characteristic drop in read density upstream of the start codon. For each bin length, we used this feature to determine the offset between the 5' read end and the P-site, and by adding 3nt to the A-site. We considered six bins (28-33 nt length) with the highest number of RPFs for calibration. Calibrated reads displayed a 3-nt periodicity indicative of genuine translation. Over all bins, the A-site codon occupancies were summed up on a transcript-specific manner and normalized on the transcript background, i.e. by the mean of randomized reads to consider differences in transcript abundance and codon frequencies across transcripts (*20*). To directly compare the differences in the ribosome dwelling occupancy (frequency) at the A-site codon between *Gars*$^{C201R/+}$ and WT control mice, the summed-up A-site codon occupancies across all transcripts for each species were then divided and presented as differential A-site codon occupancies.

Statistics

All results of statistical analysis are presented as mean ± standard error of the mean (SEM) and differences were considered significant when $p<0.05$. No statistical methods were used to pre-determine sample sizes, but our sample sizes are similar to those reported in previous publications(*9, 16*). Whenever possible, data collection and analysis were performed by investigators blinded to the genotype of the experimental animals. Animals or samples were assigned to the various experimental groups based on their genotype. For mouse experiments, littermate controls were used whenever possible. For a given experiment, samples from the different experimental groups were processed in parallel and analyzed in random order. Before analysis, a Robust regression and Outlier removal method (ROUT) was performed to detect all outliers. Normality of all data was analyzed by Shapiro–Wilk, Anderson-Darling and Kolmogorov-Smirnov tests. Subsequent statistical tests were only performed if all assumptions were met. Two-way ANOVA and subsequent Tukey's multiple comparisons test was used for

comparisons of normally distributed data of more than two groups that vary in two factors and have homogeneous variance. For normally distributed data that did not have a homogenous variance, Brown-Forsythe and Welch ANOVA was performed. To compare relative translation rates between genotypes, FUNCAT fluorescence intensities were analyzed using Brown-Forsythe and Welch ANOVA, as the number of animals per group was variable and the groups displayed unequal variance. Fisher's exact test with Bonferroni correction was used to analyze offspring frequency data and innervation status of larval muscle 24. For comparison of climbing speed, two-way ANOVA was performed when group sizes were homogeneous, and one-way ANOVA was performed when the number of animals per group were variable. Lifespan curves were analyzed using Log-Rank (Mantel-Cox) test. One-way ANOVA was used to analyze dendritic coverage of class IV MD neurons (as group sizes were heterogeneous) and $tRNA^{Gly}$ expression levels. GlyRS protein levels were analyzed using two-way ANOVA. For comparison of not normally distributed data with heterogeneous variance, a one-sample t-test (theoretical mean of control genotype) and two-tailed unpaired t-test with Bonferroni correction (to compare *Gars* mutant mice with or without $tRNA^{Gly}$ overexpression) was used per time point for the longitudinal inverted grid experiments. A two-way ANOVA with Tukey's multiple comparisons test was used to compare normally distributed balanced data for the longitudinal body weight and grip strength measurements. In case the data was unbalanced, a one-way ANOVA with Tukey's multiple comparisons test was applied. For comparison of normally distributed balanced data of EMG experiments, two-way ANOVA with Tukey's multiple comparisons test was used. In case of heterogeneous variance, a Brown-Forsythe and Welch ANOVA with Dunnett's multiple comparisons test was used. Comparisons of not normally distributed balanced data of the FISH experiments with heterogeneous variance were performed using a two-tailed Welch's t-test with Bonferroni correction. A two-way ANOVA with Tukey's multiple comparisons test was used to analyze the muscle weight measurements. A Kruskal-Wallis test with Dunn's multiple comparison test was applied to not normally distributed data of the western blot experiments. A one-sample t-test (theoretical mean of control genotype) was used to evaluate statistical significance of the amount of $tRNA^{Gly}$ co-immunoprecipitated with GlyRS from WT versus $Gars^{C201R/+}$ brain extracts. To compare motor axon numbers between genotype groups, a one-way ANOVA with Tukey's multiple comparisons test was applied. For the *Gtpbp2 x* $Gars^{C201R}$ intercross, mice heterozygous for loss of *Gtpbp2* were tested independently against wild-type using one-way ANOVA and added to wild-type *Gtpbp2* samples only after no statistical differences were found. The same was done for *n-Tr20*$^{-/-}$ versus n-*Tr20*$^{+/-}$. Finding no statistical differences with heterozygosity of *Gtpbp2* or *n-Tr20* expression, combined genotypes were then tested for significance using a one-way ANOVA test. Kolmogorov-Smirnov test was used to compare the cumulative frequency of axon diameters between genotype groups. Statistical analysis was performed using GraphPad Prism v.8.3.0.

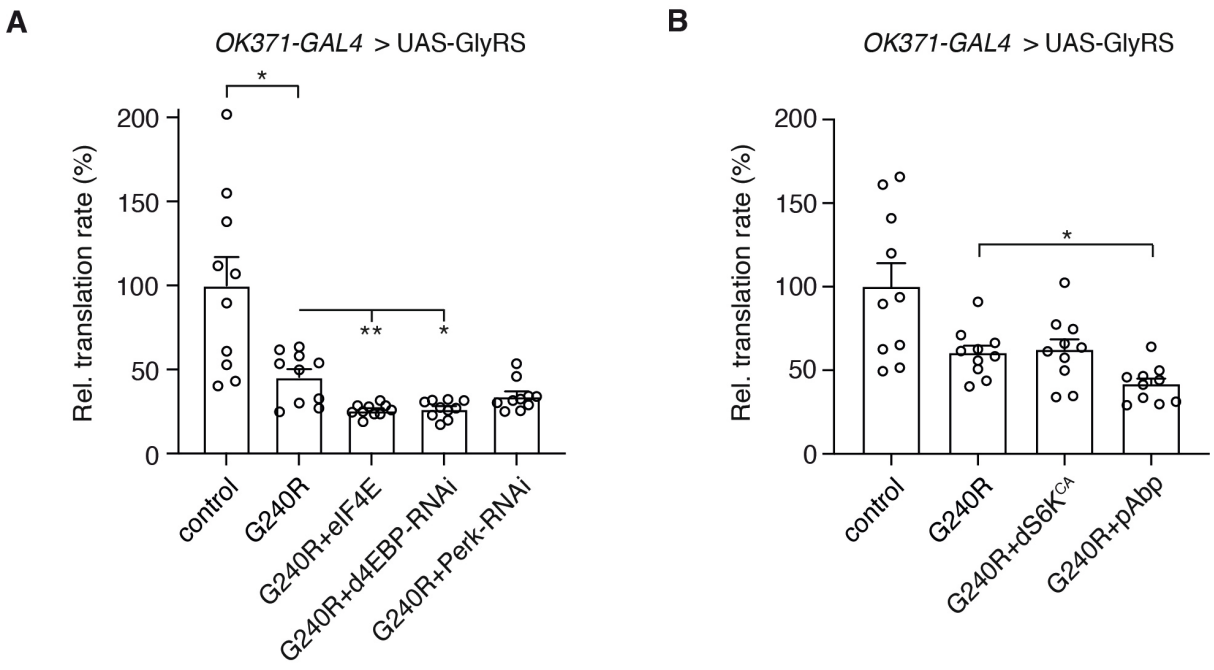

Fig. S1. Inhibition of protein synthesis by CMT-mutant GlyRS is likely not attributable to interference with upstream regulation or initiation of translation.

(**A,B**) Relative translation rates were evaluated by FUNCAT in third instar larvae that selectively expressed GlyRS-G240R in motor neurons (*OK371-GAL4*). Overexpression of eIF4E (A), constitutively active S6 kinase (dS6K^{CA}) or poly(A) binding protein (pAbp) (B), or knock-down of d4EBP or Perk (A) did not rescue the GlyRS-G240R-induced translation defect. Rather, overexpression of eIF4E (A) or pAbp (B), and knock-down of d4EBP significantly enhanced the protein synthesis defect. Control animals are driver-only. n=10 animals per genotype; *p<0.05; **p<0.01 as compared to G240R by Brown-Forsythe and Welch ANOVA. Graphs represent mean ± SEM.

Of note, each of these genetic manipulations were expected to boost translation. S6K is thought to promote mRNA translation by phosphorylating and binding multiple proteins, including eIF4B, eEF2K, SKAR, CBP80, PDCD4 and rpS6 (*43, 44*). It was previously shown that expression of constitutively active dS6K (dS6K^{STDETE}) increases tissue growth (*45*), presumably due to enhanced translation. PERK is an eIF-2α kinase. eIF2α phosphorylation occurs in response to cellular stress and results in downregulation of global translation (*6, 46*). Thus, knock-down of dPERK may reduce eIF-2α phosphorylation and enhance translation. 4EBP sequesters eukaryotic initiation factor 4E (eIF4E) from the eIF4F complex. eIF4E is the cap-binding protein, which mediates binding of eIF4F to the 5'-cap structure of mRNAs, a rate-limiting step in translation initiation (*47*). Therefore, knock-down of 4EBP is expected to boost cap-dependent translation. Poly(A)-binding protein enables the formation of a circular mRNA-protein complex, the closed-loop structure, through its interaction with the poly(A) tail and eIF4G, thereby increasing translational efficiency (*6, 48*).

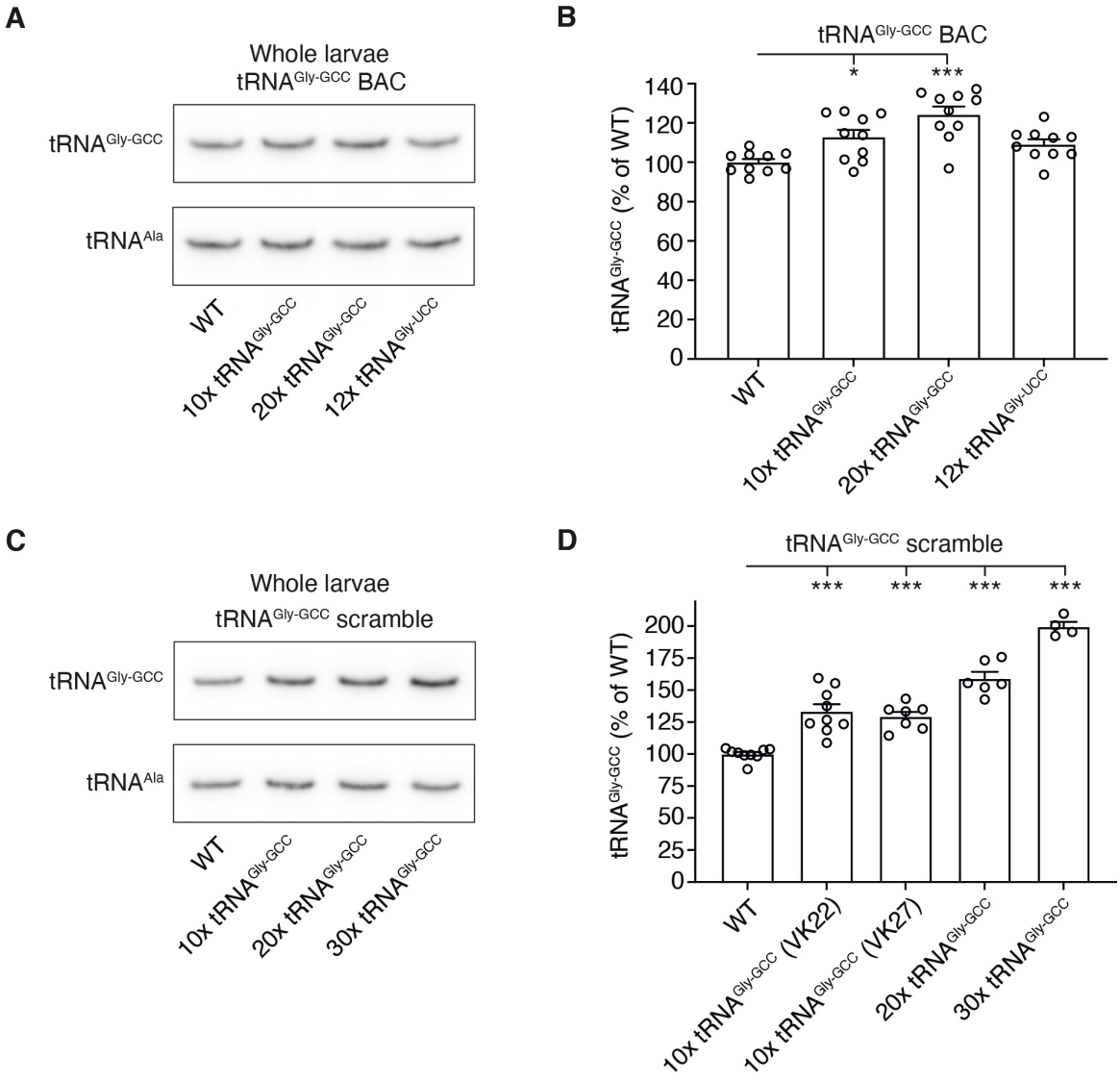

Fig. S2. Characterization of tRNA$^{Gly\text{-}GCC}$ expression levels in tRNA$^{Gly\text{-}GCC}$ transgenic Drosophila lines.

(**A**) Representative northern blot to evaluate tRNA$^{Gly\text{-}GCC}$ levels in RNA extracts from third instar whole larvae. BAC transgenic larvae containing 10 (10xtRNA$^{Gly\text{-}GCC}$) or 20 (20xtRNA$^{Gly\text{-}GCC}$) extra tRNA$^{Gly\text{-}GCC}$ gene copies were compared to wild type (WT) larvae and as an additional control transgenic larvae containing 12 extra tRNA$^{Gly\text{-}UCC}$ gene copies (12xtRNA$^{Gly\text{-}UCC}$). A probe detecting tRNA$^{Ala\text{-}AGC}$ (tRNA^{Ala}) was used as loading control. (**B**) Quantification of tRNA$^{Gly\text{-}GCC}$ levels in WT, 10xtRNA$^{Gly\text{-}GCC}$, 20xtRNA$^{Gly\text{-}GCC}$, and 12xtRNA$^{Gly\text{-}UCC}$ larvae. Data are shown as % of WT. n=10 independent samples per genotype; *p<0.05, ***p<0.0001 by one-way ANOVA with Dunnett's multiple comparisons test. (**C**) Representative northern blot to evaluate tRNA$^{Gly\text{-}GCC}$ levels in RNA extracts from third instar whole larvae. tRNA$^{Gly\text{-}GCC}$ scramble transgenic larvae containing 10 (10xtRNA$^{Gly\text{-}GCC}$), 20 (20xtRNA$^{Gly\text{-}GCC}$), or 30 (30xtRNA$^{Gly\text{-}GCC}$) extra tRNA$^{Gly\text{-}GCC}$ gene copies were compared to wild type (WT) larvae. A probe detecting tRNA$^{Ala\text{-}AGC}$ (tRNA^{Ala}) was used as loading control. (**D**) Quantification of

tRNA$^{Gly\text{-}GCC}$ levels in WT, 10xtRNA$^{Gly\text{-}GCC}$ (either VK22 or VK27 transgene insertion sites), 20xtRNA$^{Gly\text{-}GCC}$, and 30xtRNA$^{Gly\text{-}GCC}$ larvae. Data are shown as % of WT. n=4-9 independent samples per genotype; ***p<0.005 by Brown-Forsythe and Welch ANOVA with Dunnett's T3 multiple comparisons test. Graphs represent mean ± SEM.

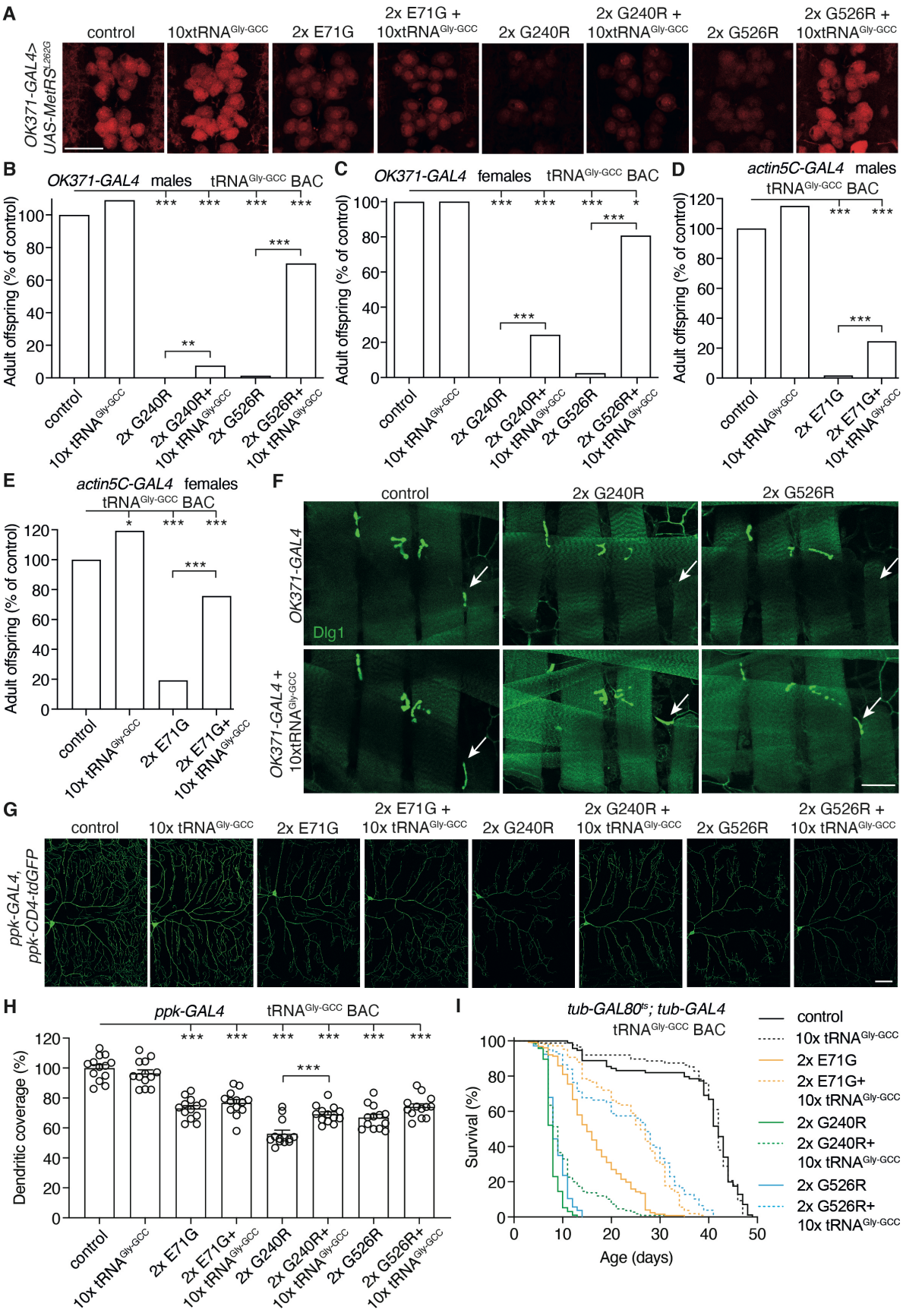
A
control
10xtRNA Gly-GCC
2x E71G
2x E71G + 10xtRNA Gly-GCC
2x G240R
2x G240R + 10xtRNA Gly-GCC
2x G526R
2x G526R + 10xtRNA Gly-GCC
OK371-GAL4> UAS-MetRS L262G
B
OK371-GAL4 males tRNA Gly-GCC BAC
Adult offspring (% of control)
control
10x tRNA Gly-GCC
2x G240R
2x G240R+ 10x tRNA Gly-GCC
2x G526R
2x G526R+ 10x tRNA Gly-GCC
C
OK371-GAL4 females tRNA Gly-GCC BAC
D
actin5C-GAL4 males tRNA Gly-GCC BAC
2x E71G
2x E71G+ 10x tRNA Gly-GCC
E
actin5C-GAL4 females tRNA Gly-GCC BAC
F
OK371-GAL4
OK371-GAL4 + 10xtRNA Gly-GCC
Dlg1
G
ppk-GAL4, ppk-CD4-tdGFP
H
ppk-GAL4 tRNA Gly-GCC BAC
Dendritic coverage (%)
I
tub-GAL80 ts; tub-GAL4 tRNA Gly-GCC BAC
Survival (%)
Age (days)

Fig. S3. tRNA$^{Gly\text{-}GCC}$ overexpression rescues peripheral neuropathy phenotypes in *Drosophila* CMT2D models.

(**A**) Representative images of *in vivo* FUNCAT in motor neurons (*OK371-GAL4> UAS-MetRS^{L262G}*) of larvae expressing E71G, G240R, or G526R GlyRS, in the presence or absence of the 10xtRNA$^{Gly\text{-}GCC}$ BAC transgene. Quantification is shown in Fig. 1B. Scale bar: 50µm. (**B,C**) Adult offspring frequency (% of driver-only control) of male (B) and female (C) flies expressing 2 copies of G240R or G526R GlyRS transgenes selectively in motor neurons (*OK371-GAL4*), in the presence or absence of the 10xtRNA$^{Gly\text{-}GCC}$ BAC transgene. n>450 F1 flies per cross; *p<0.05; **p<0.01; ***p<0.0001 by Fisher's exact test with Bonferroni correction. Note that the E71G GlyRS mutant was not included in this experiment, as motor-neuron selective GlyRS-E71G expression does not reduce adult offspring frequency (Table S1). (**D,E**) Adult offspring frequency (% of driver-only control) of male (D) and female (E) flies ubiquitously (*actin5C-GAL4*) expressing 2 copies of the GlyRS-E71G transgene, in the presence or absence of the 10xtRNA$^{Gly\text{-}GCC}$ BAC transgene. n>550 F1 flies per cross; *p<0.05; ***p<0.005 by Fisher's exact test with Bonferroni correction. (**F**) Representative images of muscle 24 innervation status in third instar larvae expressing GlyRS transgenes selectively in motor neurons (*OK371-GAL4*), in the presence or absence of the 10xtRNA$^{Gly\text{-}GCC}$ BAC transgene. NMJs were visualized using Dlg1 immunostaining. The NMJ on muscle 24 is indicated with a white arrow, illustrating that muscle 24 innervation is missing upon expression of GlyRS-G240R or G526R. This defect is rescued by tRNA$^{Gly\text{-}GCC}$ overexpression. Control is driver-only. Scale bar: 50µm. (**G,H**) Representative images (G) and quantification (H) of dendritic coverage (% of driver-only control) of class IV multidendritic sensory neurons in the larval body wall upon selective expression of GlyRS transgenes in these neurons (*ppk-GAL4*), in the presence or absence of 10xtRNA$^{Gly\text{-}GCC}$ BAC. n=13 animals per genotype; ***p<0.005 by two-way ANOVA. Graph represents mean ± SEM. Scale bar: 50µm. (**I**) Life span of flies ubiquitously expressing GlyRS transgenes from the adult stage onwards (*tub-GAL80^{ts}; tub-GAL4*), in the presence or absence of 10xtRNA$^{Gly\text{-}GCC}$ BAC. Control flies are driver-only. n=79-126 flies per genotype; p<0.0005 for each GlyRS mutant versus GlyRS mutant + 10xtRNA$^{Gly\text{-}GCC}$ by Log-rank (Mantel-Cox) test.

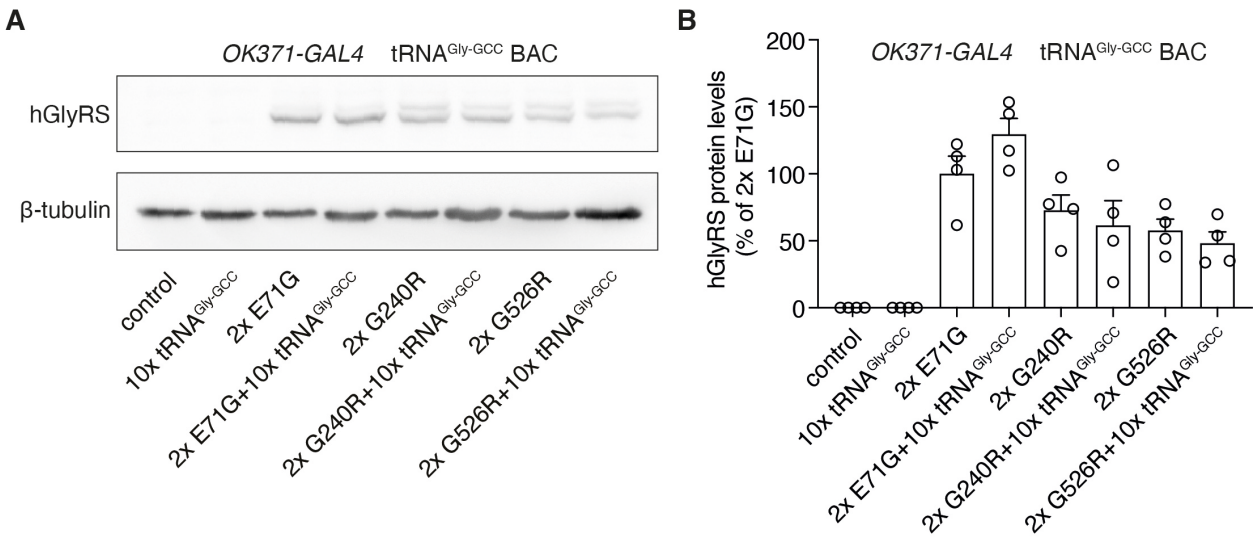

Fig. S4. tRNA$^{Gly-GCC}$ overexpression does not affect expression levels of CMT-mutant GlyRS proteins.

(**A**) Representative western blot to evaluate human GlyRS (hGlyRS) protein levels in the CNS of third instar larvae selectively expressing E71G, G240R, or G526R GlyRS proteins in motor neurons (*OK371-GAL4*), in the presence or absence of the 10xtRNA$^{Gly-GCC}$ BAC transgene. Control is driver-only. β-tubulin was used as loading control. The lower (darker) hGlyRS bands were used for quantification. (**B**) Quantification of GlyRS protein levels in the CNS of third instar larvae selectively expressing E71G, G240R, or G526R GlyRS proteins in motor neurons (*OK371-GAL4*), in the presence or absence of 10xtRNA$^{Gly-GCC}$ BAC. Data are shown as % of 2x E71G. n=4 independent samples per genotype; p=ns for genotypes with or without 10xtRNA$^{Gly-GCC}$ by two-way ANOVA. Graph represents mean ± SEM.

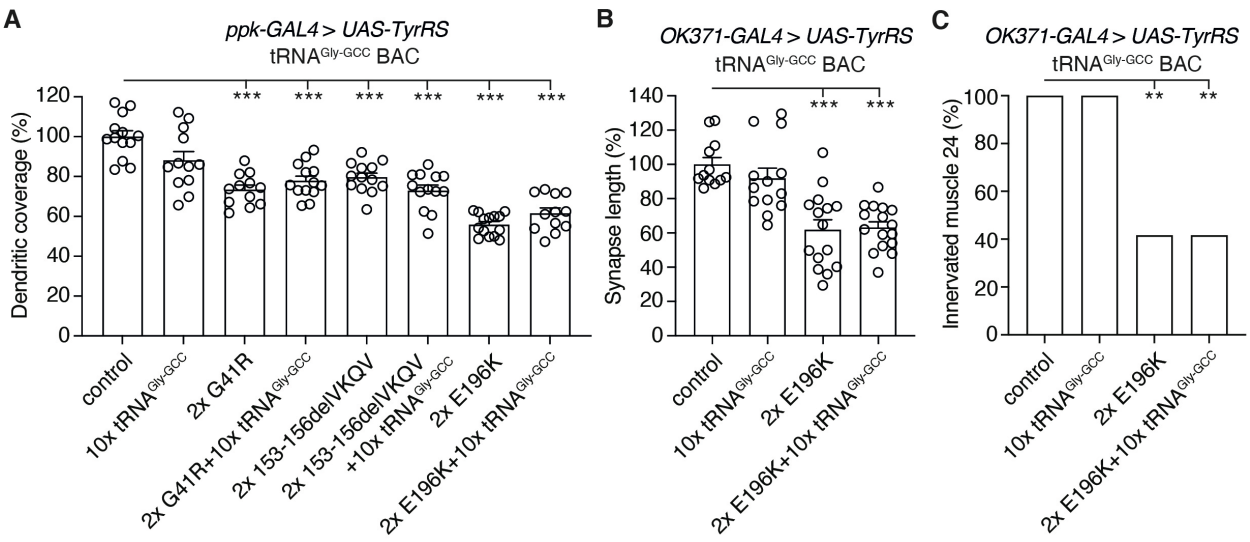

Fig. S5. tRNA$^{Gly\text{-}GCC}$ overexpression does not rescue phenotypes induced by CMT-mutant TyrRS.

(**A**) Dendritic coverage (% of driver-only control) of class IV multidendritic sensory neurons in the larval body wall. Reduced dendritic coverage induced by selective expression of G41R, 153-156delVKQV, or E196K TyrRS in these sensory neurons (*ppk-GAL4*) was not affected by tRNA$^{Gly\text{-}GCC}$ overexpression. n=12-14 animals per genotype; ***p<0.0001 by Brown-Forsythe and Welch ANOVA with Dunnett's T3 multiple comparisons test. **(B)** Synapse length on distal muscle 8 of larvae selectively expressing TyrRS-E196K in motor neurons (*OK371-GAL4*), in the presence or absence of 10xtRNA$^{Gly\text{-}GCC}$ BAC. Control flies are driver-only. n=12-16 animals per genotype; ***p<0.0001 by one-way ANOVA with Sidak's multiple comparisons test. **(C)** Percentage of larvae with innervated muscle 24. Denervation of muscle 24 induced by selective expression of TyrRS-E196K in motor neurons (*OK371-GAL4*) was not affected by tRNA$^{Gly\text{-}GCC}$ overexpression. n=12 animals per genotype; **p<0.01 by Fisher's exact test with Bonferroni correction. Graphs represent mean ± SEM.

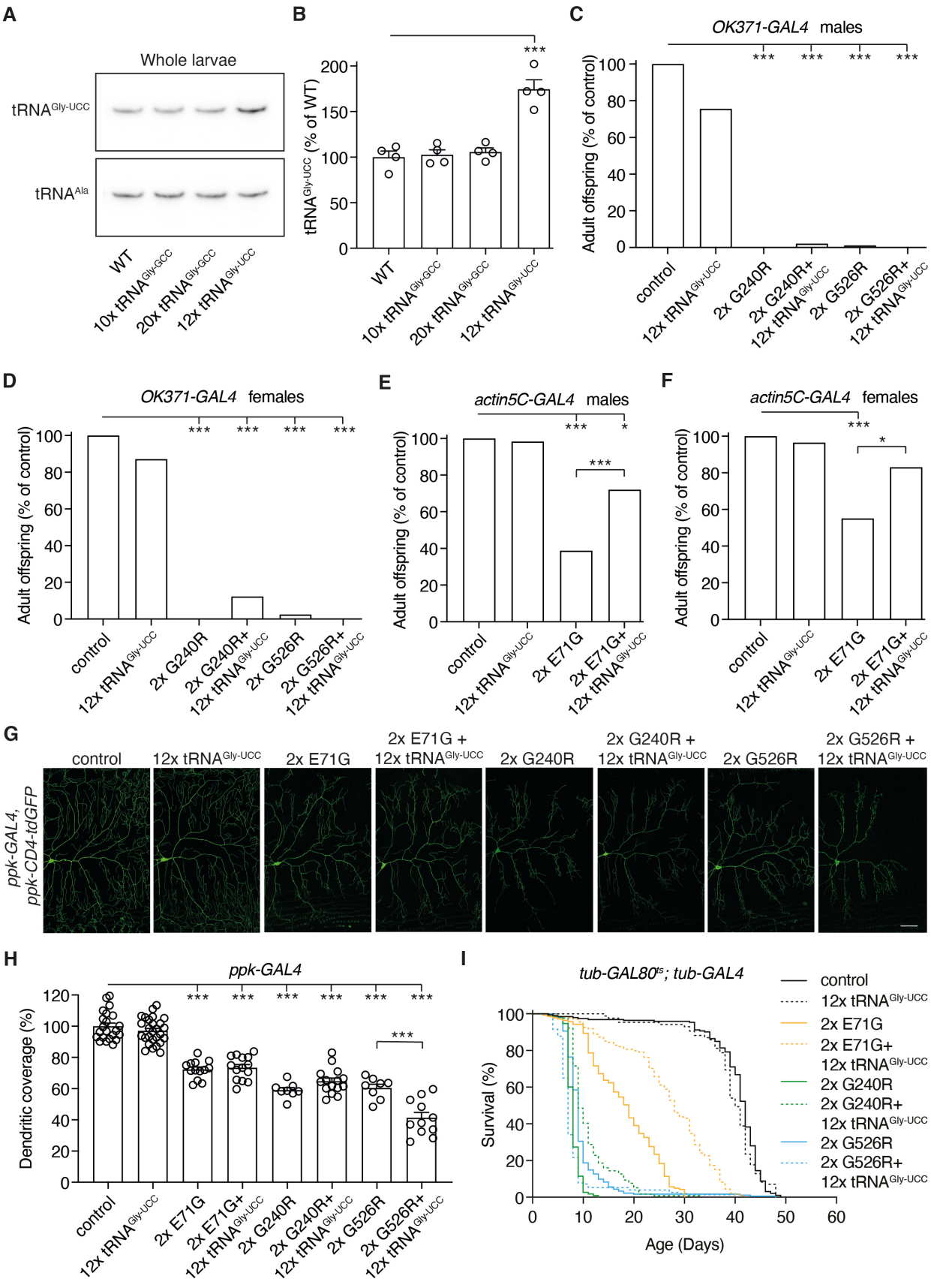
A
Whole larvae
tRNA Gly-UCC
tRNA Ala
WT
10x tRNA Gly-GCC
20x tRNA Gly-GCC
12x tRNA Gly-UCC
B
tRNA Gly-UCC (% of WT)
***
C
OK371-GAL4 males
Adult offspring (% of control)
control
12x tRNA Gly-UCC
2x G240R
2x G240R+ 12x tRNA Gly-UCC
2x G526R
2x G526R+ 12x tRNA Gly-UCC
D
OK371-GAL4 females
E
actin5C-GAL4 males
2x E71G
2x E71G+ 12x tRNA Gly-UCC
F
actin5C-GAL4 females
G
control
12x tRNA Gly-UCC
2x E71G
2x E71G + 12x tRNA Gly-UCC
2x G240R
2x G240R + 12x tRNA Gly-UCC
2x G526R
2x G526R + 12x tRNA Gly-UCC
ppk-GAL4, ppk-CD4-tdGFP
H
ppk-GAL4
Dendritic coverage (%)
I
tub-GAL80ts; tub-GAL4
Survival (%)
Age (Days)

Fig. S6. Effect of tRNA$^{Gly-UCC}$ overexpression on peripheral neuropathy phenotypes in *Drosophila* CMT2D models.

(**A**) Representative northern blot to evaluate tRNA$^{Gly-UCC}$ levels in RNA extracts from third instar whole larvae. 12xtRNA$^{Gly-UCC}$ transgenic larvae were compared to WT and as additional controls 10xtRNA$^{Gly-GCC}$ and 20xtRNA$^{Gly-GCC}$ BAC transgenic larvae. A probe detecting tRNA$^{Ala-AGC}$ (tRNA^{Ala}) was used as loading control. (**B**) Quantification of tRNA$^{Gly-UCC}$ levels in WT, 10xtRNA$^{Gly-GCC}$, 20xtRNA$^{Gly-GCC}$ and 12xtRNA$^{Gly-UCC}$ larvae. Data are shown as % of WT. n=4 independent samples per genotype. ***p<0.0001 by one-way ANOVA. (**C,D**) Adult offspring frequency (% of driver-only control) of male (C) and female (D) flies expressing 2 copies of GlyRS-G240R or GlyRS-G526R transgenes selectively in motor neurons (*OK371-GAL4*), in the presence or absence of 12xtRNA$^{Gly-UCC}$. n>300 F1 flies per cross; ***p<0.0001 by Fisher's exact test with Bonferroni correction. (**E,F**) Adult offspring frequency (% of driver-only control) of male (E) and female (F) flies ubiquitously (*actin5C-GAL4*) expressing 2 copies of the GlyRS-E71G transgene, in the presence or absence of 12xtRNA$^{Gly-UCC}$. n>285 F1 flies per cross; *p<0.05; ***p<0.005 by Fisher's exact test with Bonferroni correction. (**G,H**) Representative images (G) and quantification (H) of dendritic coverage (% of driver-only control) of class IV multidendritic sensory neurons, in which GlyRS transgenes were selectively expressed (*ppk-GAL4*), in the presence or absence of 12xtRNA$^{Gly-UCC}$. n=8-27 animals per genotype; ***p<0.0001 by one-way ANOVA. Scale bar: 50µm. (**I**) Life span of flies ubiquitously expressing GlyRS transgenes from the adult stage onwards (*GAL80^{ts}; tub-GAL4*), in the presence or absence of 12xtRNA$^{Gly-UCC}$. Control flies are driver-only. n=85-193 flies per genotype; p<0.0001 for each GlyRS mutant versus GlyRS mutant + 12xtRNA$^{Gly-UCC}$ by Log-rank (Mantel-Cox) test. Graphs represent mean ± SEM.

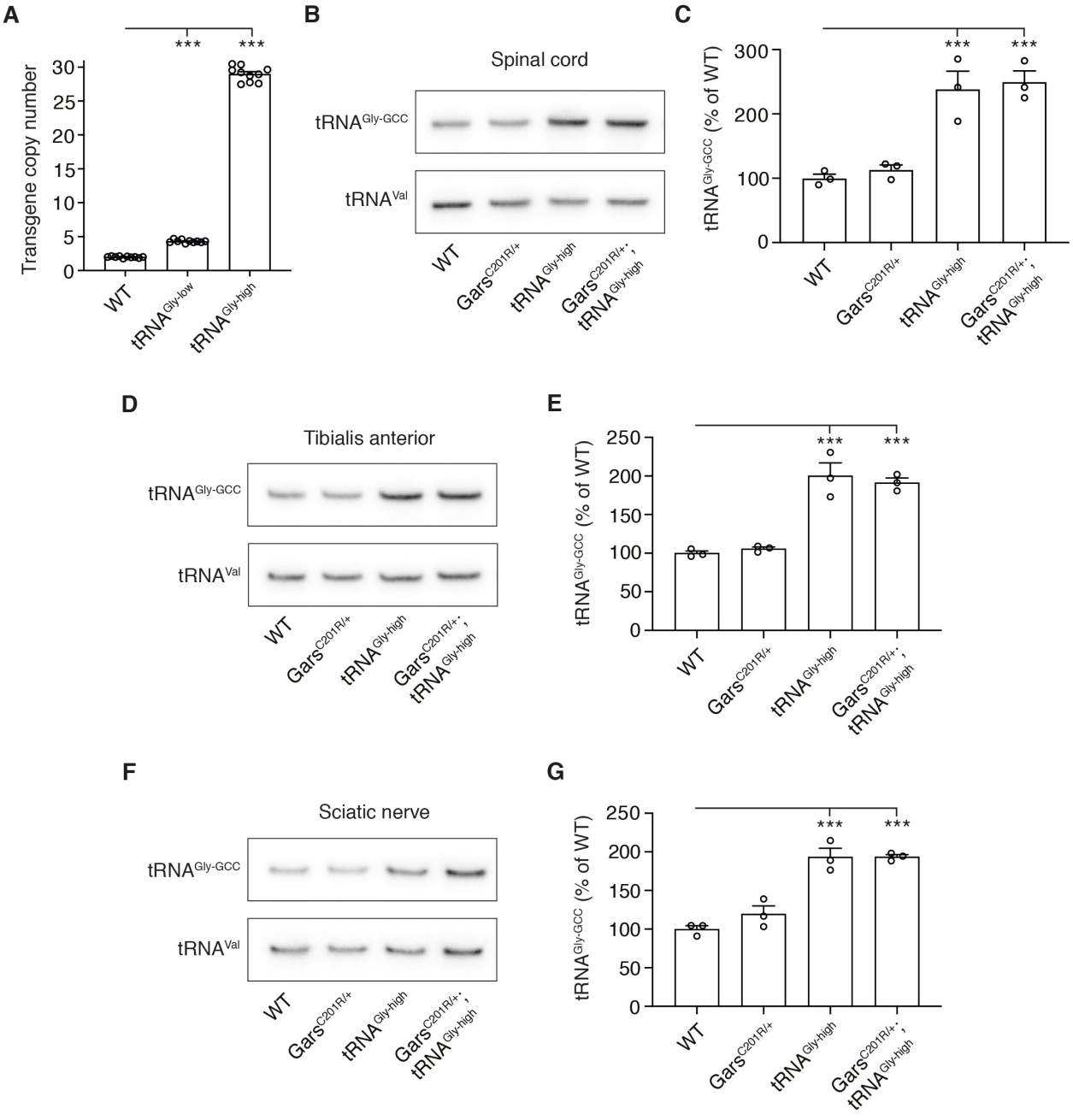

Fig. S7. Characterization of tRNA$^{Gly\text{-}GCC}$ transgenic mice.

(**A**) Copy number analysis revealed an estimated transgene copy number of 2 for tRNA$^{Gly\text{-}low}$ and 27 for tRNA$^{Gly\text{-}high}$ mice. This corresponds to 4 and 54 additional tRNA$^{Gly\text{-}GCC}$ gene copies, respectively. n=10 mice per genotype; ***p<0.0001 by Brown-Forsythe and Welch ANOVA. (**B,D,F**) Representative northern blots to evaluate tRNA$^{Gly\text{-}GCC}$ levels in spinal cord (B), tibialis anterior (D), and sciatic nerve (F) of WT, *Gars*$^{C201R/+}$, tRNA$^{Gly\text{-}high}$, and *Gars*$^{C201R/+}$; tRNA$^{Gly\text{-}high}$ mice. A probe detecting tRNA$^{Val\text{-}CAC}$ (tRNA^{Val}) was used as loading control. (**C,E,G**) Quantification of tRNA$^{Gly\text{-}GCC}$ levels in spinal cord (C), tibialis anterior (E), and sciatic nerve (G), as evaluated by northern blotting. Data are shown as % of WT. n=3 mice per genotype;

***p<0.005 by two-way ANOVA with Tukey's multiple comparisons test. Graphs represent mean ± SEM.

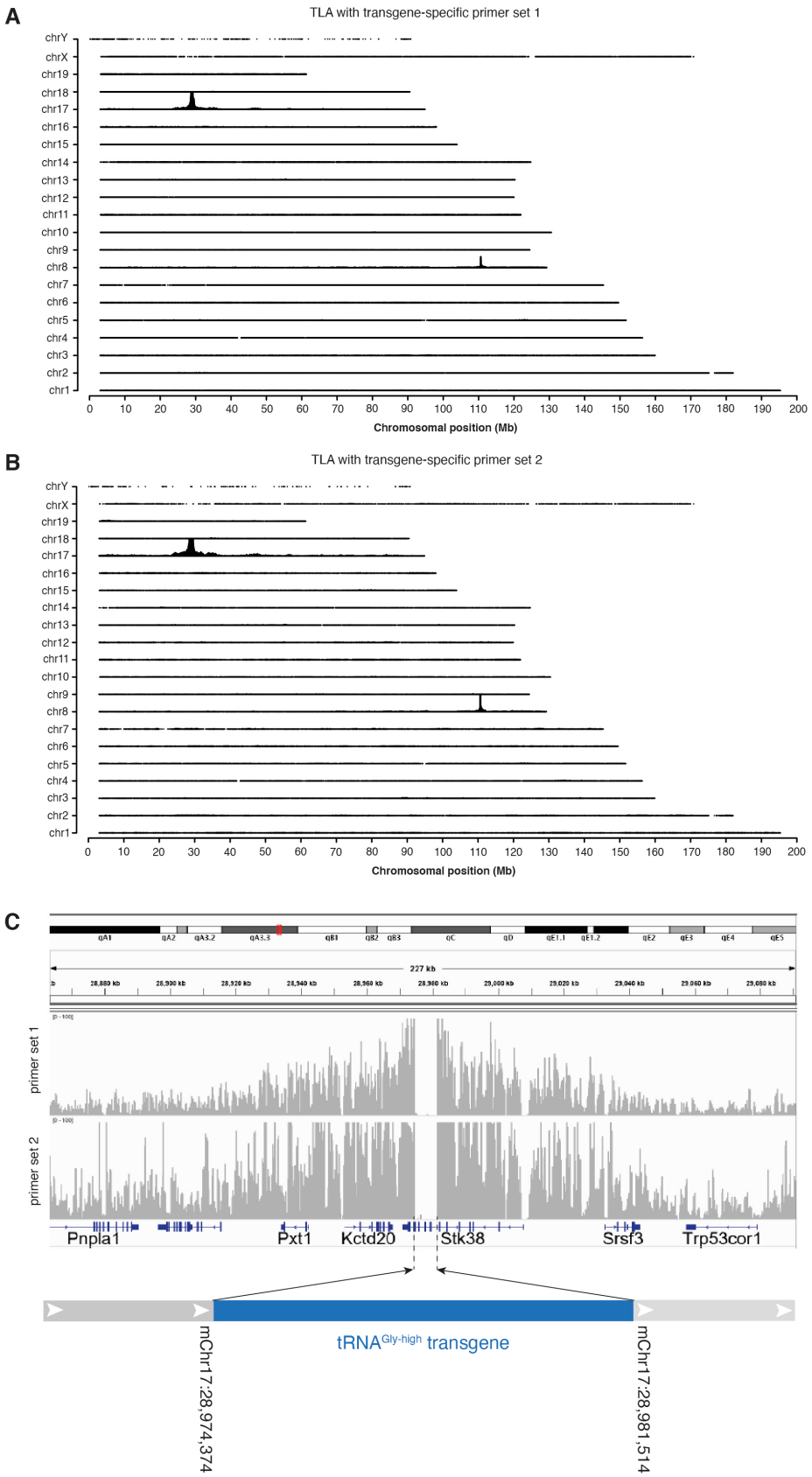
A
TLA with transgene-specific primer set 1
chrY
chrX
chr19
chr18
chr17
chr16
chr15
chr14
chr13
chr12
chr11
chr10
chr9
chr8
chr7
chr6
chr5
chr4
chr3
chr2
chr1
0 10 20 30 40 50 60 70 80 90 100 110 120 130 140 150 160 170 180 190 200
Chromosomal position (Mb)
B
TLA with transgene-specific primer set 2
chrY
chrX
chr19
chr18
chr17
chr16
chr15
chr14
chr13
chr12
chr11
chr10
chr9
chr8
chr7
chr6
chr5
chr4
chr3
chr2
chr1
0 10 20 30 40 50 60 70 80 90 100 110 120 130 140 150 160 170 180 190 200
Chromosomal position (Mb)
C
227 kb
primer set 1
primer set 2
Pnpla1
Pxt1
Kctd20
Stk38
Srsf3
Trp53cor1
tRNAGly-high transgene
mChr17:28,974,374
mChr17:28,981,514

Fig. S8. Insertion site of the tRNA$^{Gly\text{-}high}$ transgene on chromosome 17.

(**A,B**) TLA sequence coverage obtained with two independent transgene-specific primer sets. Mouse chromosomes 1 through Y are arranged on the Y-axis. X-axis shows chromosomal position. (**C**) Detailed view of TLA sequence coverage surrounding the transgene integration site. Upper and lower sequence coverage plots were obtained with transgene-specific primer sets 1 and 2, respectively. Lower panel: graphic representation of transgene insertion site. Gray: flanking genomic sequence. Blue: tRNA$^{Gly\text{-}high}$ transgene. Only one transgene copy is shown for simplicity.

TLA revealed that in tRNA$^{Gly\text{-}high}$ mice all transgene copies are integrated in the same site on chromosome 17, and a genomic deletion of ~7kb between the breakpoints of the integration site was uncovered which deletes exons 8-12 of the *Stk38* gene. *Stk38* encodes serine/threonine kinase 38, also known as Nuclear Dbf-related kinase 1 (NDR1). NDR1 kinase is known to mediate apoptosis downstream of the mammalian Ste-20-like kinase (MST1) (*49*). NDR1 is expressed at high levels in spleen, lung and thymus (*50*), and ablation of Stk38/NDR1 in mice predisposes mice to cancer as a result of compromised apoptosis (*51*).

The 7kb genomic deletion removing exons 8-12 of the *Stk38* gene is expected to inactivate this gene. However, given the fact that heterozygous tRNA$^{Gly\text{-}high}$ mice were used in this study, and that there is no known link between the *Stk38* gene and peripheral neuropathy, protein synthesis or the integrated stress response, it is highly unlikely that inactivation of one copy of this gene would be responsible for the full phenotypic rescue of *Gars*$^{C201R/+}$ mice.

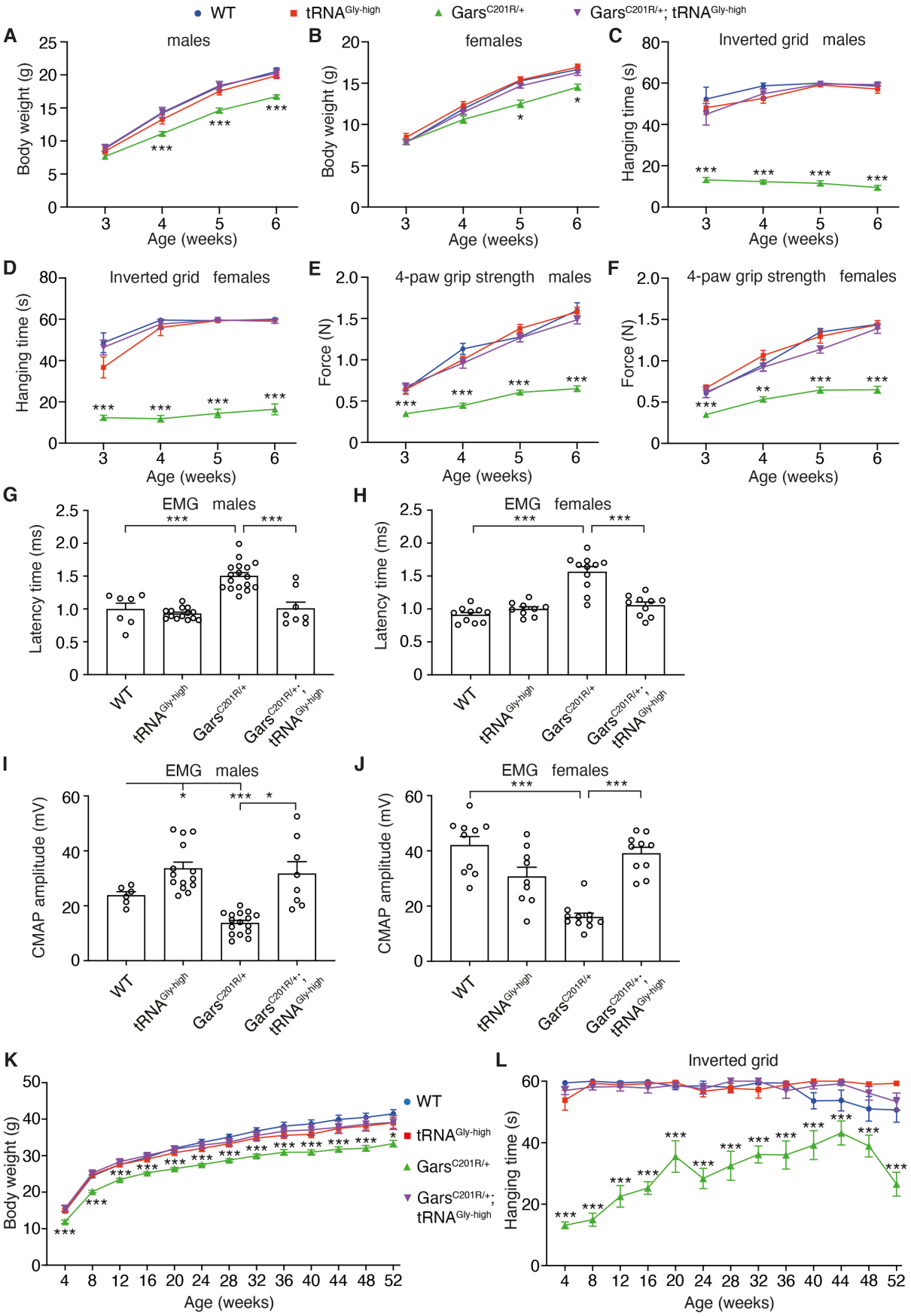
WT
tRNA Gly-high
Gars C201R/+
Gars C201R/+; tRNA Gly-high
A
males
Body weight (g)
Age (weeks)
B
females
C
Inverted grid males
Hanging time (s)
D
Inverted grid females
E
4-paw grip strength males
Force (N)
F
4-paw grip strength females
G
EMG males
Latency time (ms)
H
EMG females
I
EMG males
CMAP amplitude (mV)
J
EMG females
K
L
Inverted grid

Fig. S9. tRNA$^{Gly\text{-}GCC}$ overexpression rescues peripheral neuropathy in *Gars*$^{C201R/+}$ mice. (**A,B**) Body weight of a cohort of male (A) and female (B) WT, tRNA$^{Gly\text{-}high}$, *Gars*$^{C201R/+}$, and *Gars*$^{C201R/+}$; tRNA$^{Gly\text{-}high}$ littermate mice at 3, 4, 5, and 6 weeks of age. n=7-17 (A) and 9-11 (B) mice per genotype; *p<0.05; ***p<0.005 by Kruskal-Wallis test with Dunn's multiple comparisons test per time point. (**C,D**) Hanging time of the same cohort of mice in the inverted grid test. n=7-17 (C) and 9-11 (D) mice per genotype; ***p<0.0005 by one-sample t-test (theoretical mean of WT) and two-tailed unpaired t-test with Bonferroni correction per time point. (**E,F**) 4-paw grip strength of the same cohort of mice as measured by dynamometer. n=7-17 (E) and 9-11 (F) mice per genotype; **p<0.01; ***p<0.005 by Kruskal-Wallis test with Dunn's multiple comparisons test per time point. (**G-J**) Analysis of the same cohort of mice at 5 weeks of age by electromyography (EMG). (G,H) Latency time between stimulation of the sciatic nerve at the sciatic notch level and detection of a compound muscle action potential (CMAP) in the gastrocnemius muscle. n=7-17 (G) and 9-11 (H) mice per genotype; ***p<0.005 by Brown-Forsythe and Welch ANOVA. (I,J) CMAP amplitude in the gastrocnemius muscle. n=7-17 (I) and 9-11 (J) mice per genotype; *p<0.05; ***p<0.0005 by Brown-Forsythe and Welch ANOVA. (**K,L**) Body weight (K) and hanging time in the inverted grid test (L) of a cohort of male WT, tRNA$^{Gly\text{-}high}$, *Gars*$^{C201R/+}$, and *Gars*$^{C201R/+}$; tRNA$^{Gly\text{-}high}$ littermate mice from 4 until 52 weeks of age. n=10-11 mice per genotype; *p<0.05; ***p<0.005 by two-way ANOVA with Tukey's multiple comparisons test per time point (K) or one-sample t-test (theoretical mean of WT) and two-tailed unpaired t-test per time point (L). Graphs represent mean ± SEM.

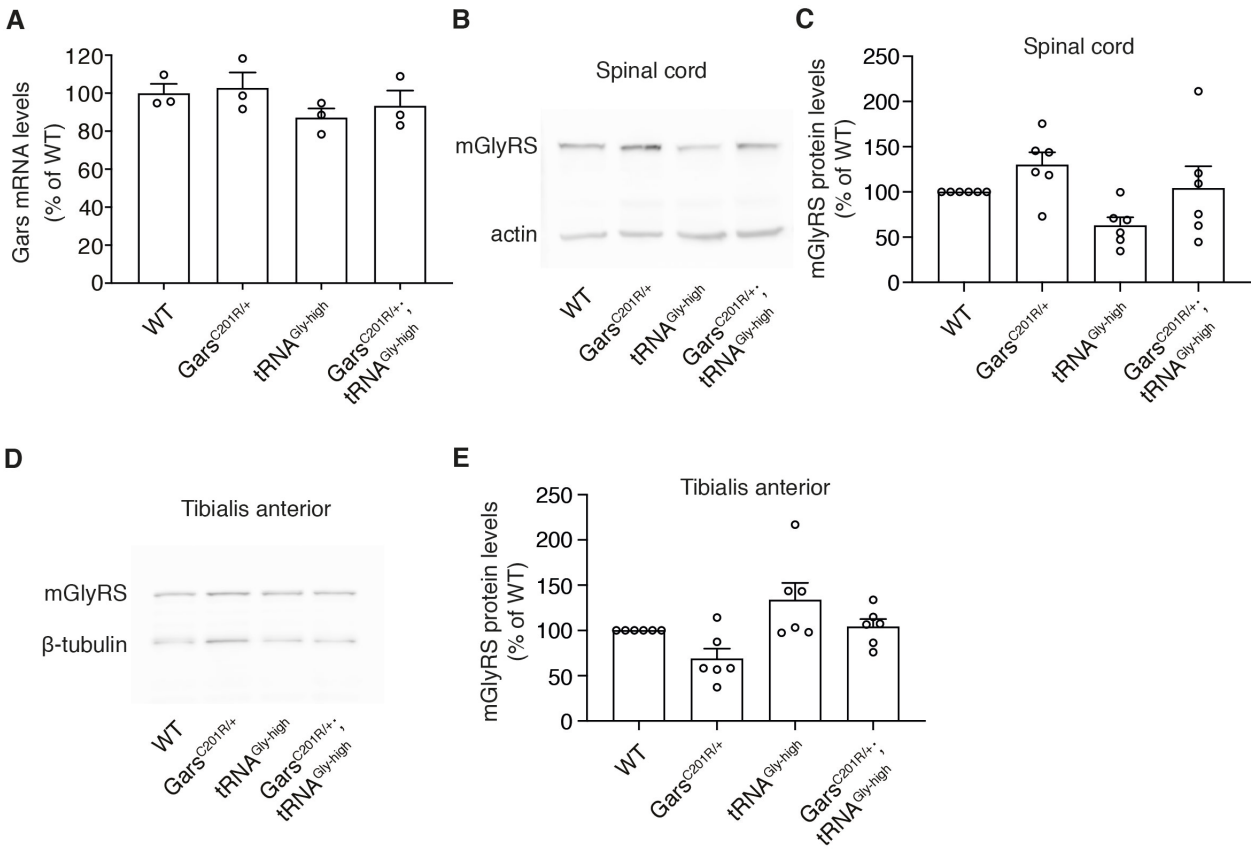

Fig. S10. tRNA$^{Gly\text{-}GCC}$ overexpression does not affect *Gars* mRNA and GlyRS protein levels. (**A**) *Gars* mRNA expression levels in spinal cord of WT, *Gars*$^{C201R/+}$, tRNA$^{Gly\text{-}high}$, and *Gars*$^{C201R/+}$; tRNA$^{Gly\text{-}high}$ littermate mice at 6 weeks of age. n=3; p=ns by two-way ANOVA with Tukey's multiple comparisons test. (**B,D**) Representative western blots to evaluate murine GlyRS (mGlyRS) protein levels in the spinal cord (B) or tibialis anterior (D) of WT, *Gars*$^{C201R/+}$, tRNA$^{Gly\text{-}high}$, and *Gars*$^{C201R/+}$; tRNA$^{Gly\text{-}high}$ mice at 12 weeks of age. Actin (B) or β-tubulin (D) was used as loading control. **(C,E)** Quantification of mGlyRS protein levels in spinal cord (C) or tibialis anterior (E) of WT, *Gars*$^{C201R/+}$, tRNA$^{Gly\text{-}high}$, and *Gars*$^{C201R/+}$; tRNA$^{Gly\text{-}high}$ mice at 12 weeks of age. Data are shown as % of WT. n=6 mice per genotype; p=ns by Kruskal-Wallis test. Graphs represent mean ± SEM.

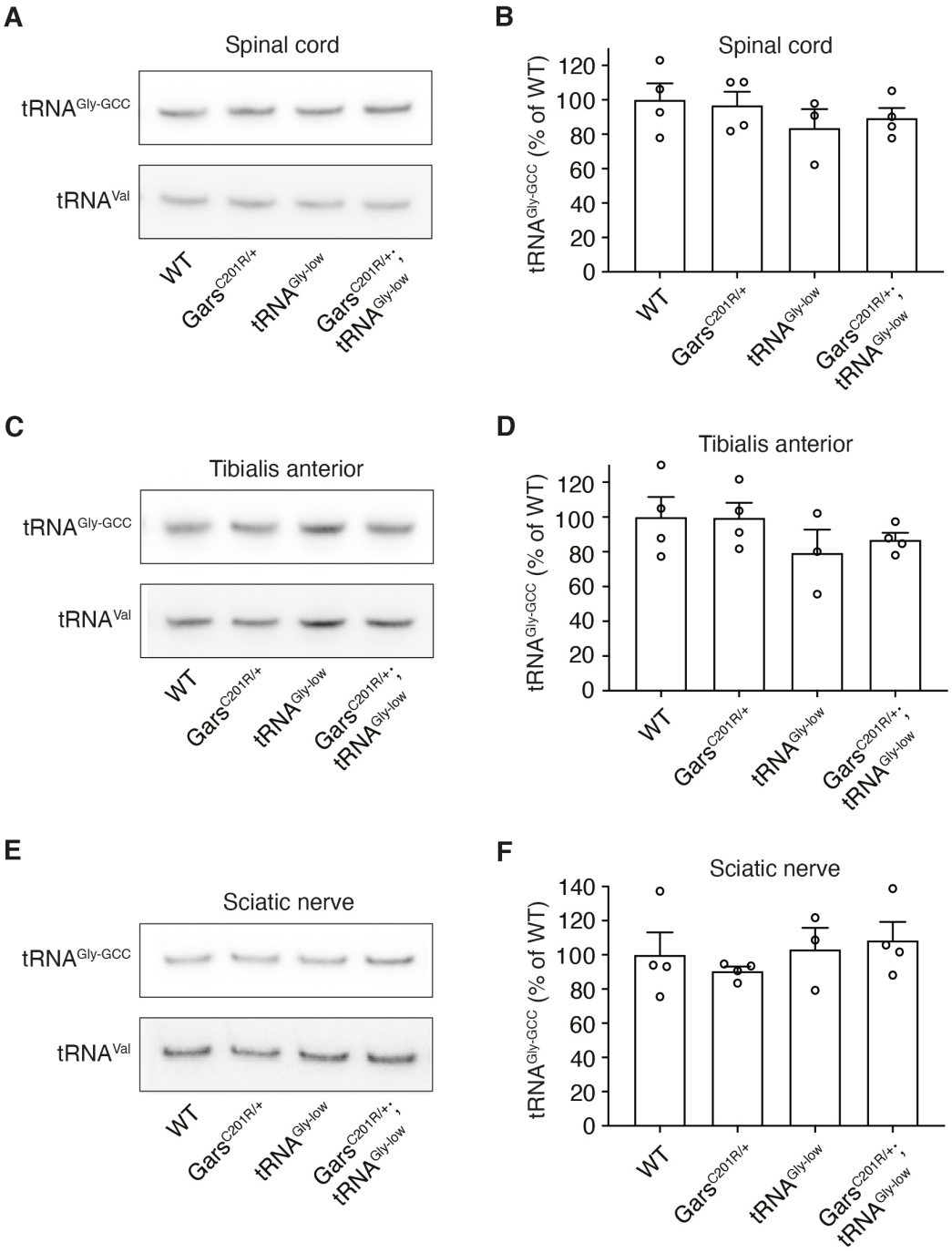

Fig. S11. No detectable tRNA$^{Gly\text{-}GCC}$ overexpression in tRNA$^{Gly\text{-}low}$ mice.

(**A,C,E**) Representative northern blots to evaluate tRNA$^{Gly\text{-}GCC}$ levels in spinal cord (A), tibialis anterior (C), and sciatic nerve (E) of WT, *Gars*$^{C201R/+}$, tRNA$^{Gly\text{-}low}$, and *Gars*$^{C201R/+}$; tRNA$^{Gly\text{-}low}$ mice. A probe detecting tRNA$^{Val\text{-}CAC}$ (tRNA^{Val}) was used as loading control. (**B,D,F**) Quantification of tRNA$^{Gly\text{-}GCC}$ levels in spinal cord (B), tibialis anterior (D), and sciatic nerve (F), as evaluated by northern blotting. Data are shown as % of WT. n=3-4 mice per genotype; p=ns by two-way ANOVA with Tukey's multiple comparisons test. Graphs represent mean ± SEM.

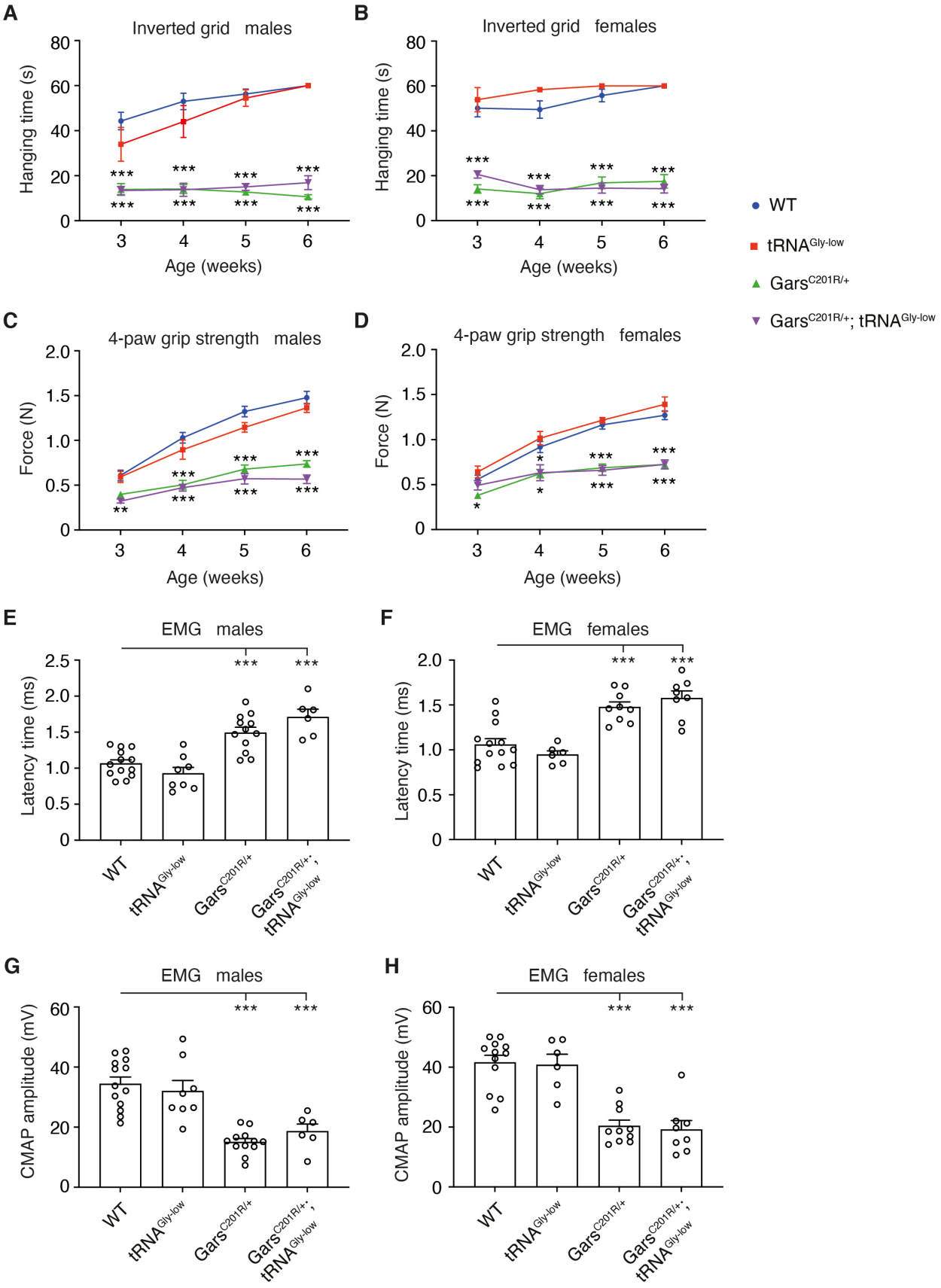
A
Inverted grid males
Hanging time (s)
Age (weeks)
B
Inverted grid females
Hanging time (s)
Age (weeks)
C
4-paw grip strength males
Force (N)
Age (weeks)
D
4-paw grip strength females
Force (N)
Age (weeks)
E
EMG males
Latency time (ms)
F
EMG females
Latency time (ms)
G
EMG males
CMAP amplitude (mV)
H
EMG females
CMAP amplitude (mV)
WT
tRNA Gly-low
Gars C201R/+
Gars C201R/+; tRNA Gly-low

Fig. S12. The tRNA$^{Gly\text{-}low}$ transgene does not rescue peripheral neuropathy in *Gars*$^{C201R/+}$ mice.

(**A,B**) Hanging time in the inverted grid test of a cohort of male (A) and female (B) WT, tRNA$^{Gly\text{-}low}$, *Gars*$^{C201R/+}$, and *Gars*$^{C201R/+}$; tRNA$^{Gly\text{-}low}$ littermate mice at 3, 4, 5, and 6 weeks of age. n=6-13 mice per genotype; ***p<0.0001 by one-sample t-test (theoretical mean of WT) and two-tailed unpaired t-test with Bonferroni correction per time point. (**C,D**) 4-paw grip strength of the same cohort of mice as measured by dynamometer. n=6-13 mice per genotype; *p<0.05; **p<0.01; ***p<0.005 by Kruskal-Wallis test with Dunn's multiple comparisons test per time point (C) or one-way ANOVA with Tukey's multiple comparisons test per time point (D). (**E-H**) Analysis of the same cohort of mice at 5 weeks of age by electromyography (EMG). (E,F) Latency time between stimulation of the sciatic nerve at the sciatic notch level and detection of a CMAP in the gastrocnemius muscle. n=6-13 mice per genotype; ***p<0.0005 by one-way ANOVA with Tukey's multiple comparisons test. (G,H) CMAP amplitude in the gastrocnemius muscle. n=6-13 mice per genotype; ***p<0.005 by one-way ANOVA with Sidak's multiple comparisons test. Graphs represent mean ± SEM.

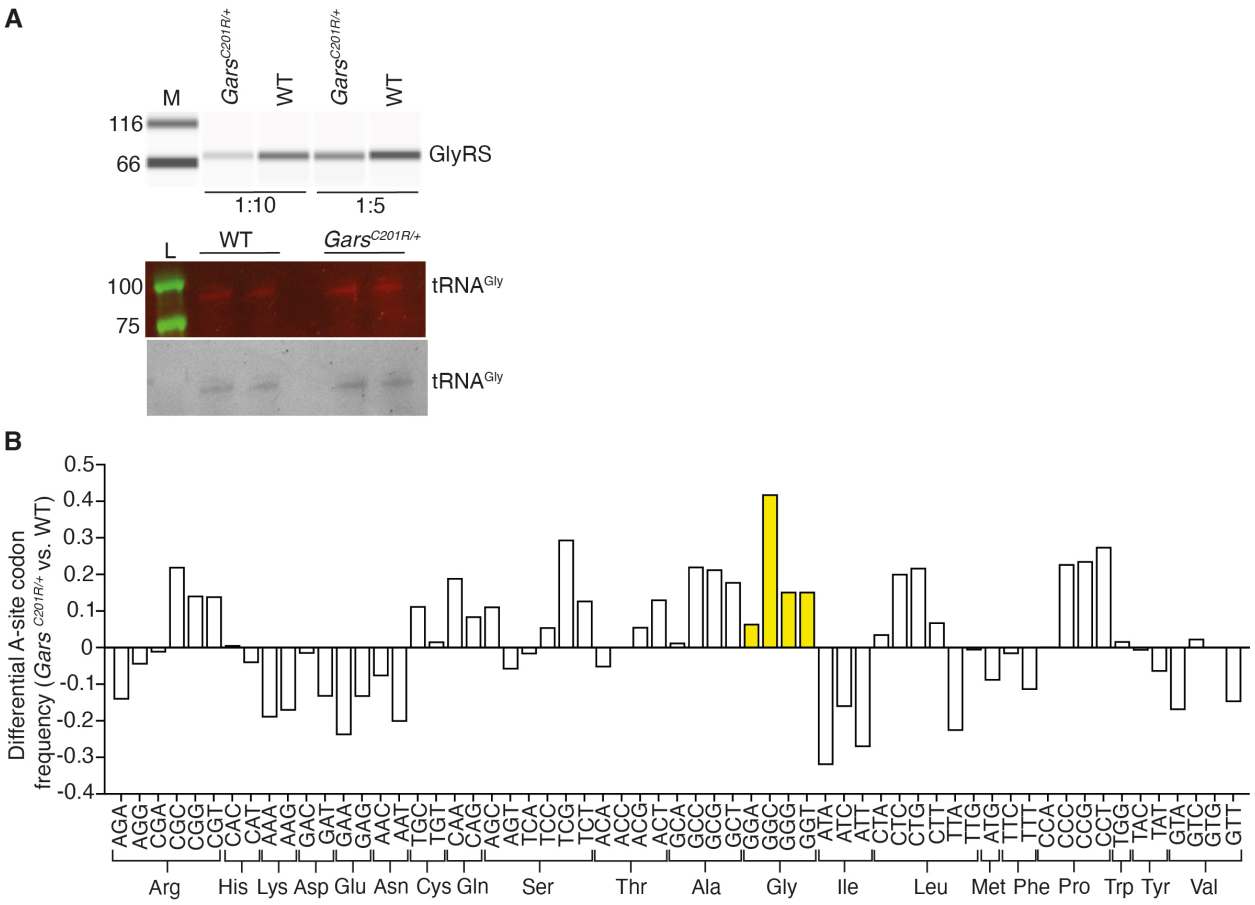

Fig. S13. Ribosome stalling on Gly codons contributes to peripheral neuropathy phenotypes in *Gars*$^{C201R/+}$ mice.

(**A**) Example of quantification of tRNA^{Gly} bound to GlyRS in complexes immunoprecipitated from whole brains of *Gars*$^{C201R/+}$ and WT control mice. The amount of GlyRS was determined in two dilutions (1:5 and 1:10, upper panel) using a capillary electrophoresis immunoblotting system (Jess, ProteinSimple). GlyRS-bound tRNAGly was quantified following ligation with a fluorescent oligonucleotide, loaded onto two lanes and separated on 10% denaturing polyacrylamide gel (middle panel). The quantification was performed in black-white mode (lower panel). M, protein marker; L, prestained DynaMarker for small RNAs (BioDynamics Laboratory Inc, Japan). (**B**) Relative changes in ribosome dwelling occupancy (frequency) at A-site codons in spinal cord of *Gars*$^{C201R/+}$ versus WT littermate mice, as determined by ribosome profiling. The A-site frequency was separately determined for *Gars*$^{C201R/+}$ and WT mice, normalized to the transcriptome codon frequencies, and presented as a ratio to visualize the effect of the C201R mutation on A-site codon frequencies. The four Gly codons are highlighted in yellow, which in mouse are read by three tRNA isoacceptors, i.e. tRNA$^{Gly\text{-}GCC}$ for GGC and GGU codons, tRNA$^{Gly\text{-}UCC}$ for GGA and GGG, and tRNA$^{Gly\text{-}CCC}$ for GGG. Ribosome dwelling occupancy at Gly codons in the A site is elevated in *Gars*$^{C201R/+}$ spinal cord, most prominently for the GCC codon. Note that among the Gly codons, GGC is the most frequently used. This suggests increased times for binding of glycyl-tRNA^{Gly}-containing ternary complexes, consistent with paucity of charged tRNA^{Gly} in *Gars*$^{C201R/+}$ spinal cord. Note that the A-site ribosome dwelling occupancy for some codons encoding Pro, Leu, Ser, Arg and Ala are also elevated. It

was previously reported that perturbation of aminoacylation of one tRNA family can affect aminoacylation levels of other tRNA families (*52, 53*) through a hitherto unknown molecular mechanism. The relatively modest increase of Gly codon frequency in the ribosomal A site may be attributable to the fact that ribosome stalling may predominantly or even selectively occur in motor neurons of *Gars*$^{C201R/+}$ mice, as suggested by the selective activation of the integrated stress response in motor neurons (Fig. S15G).

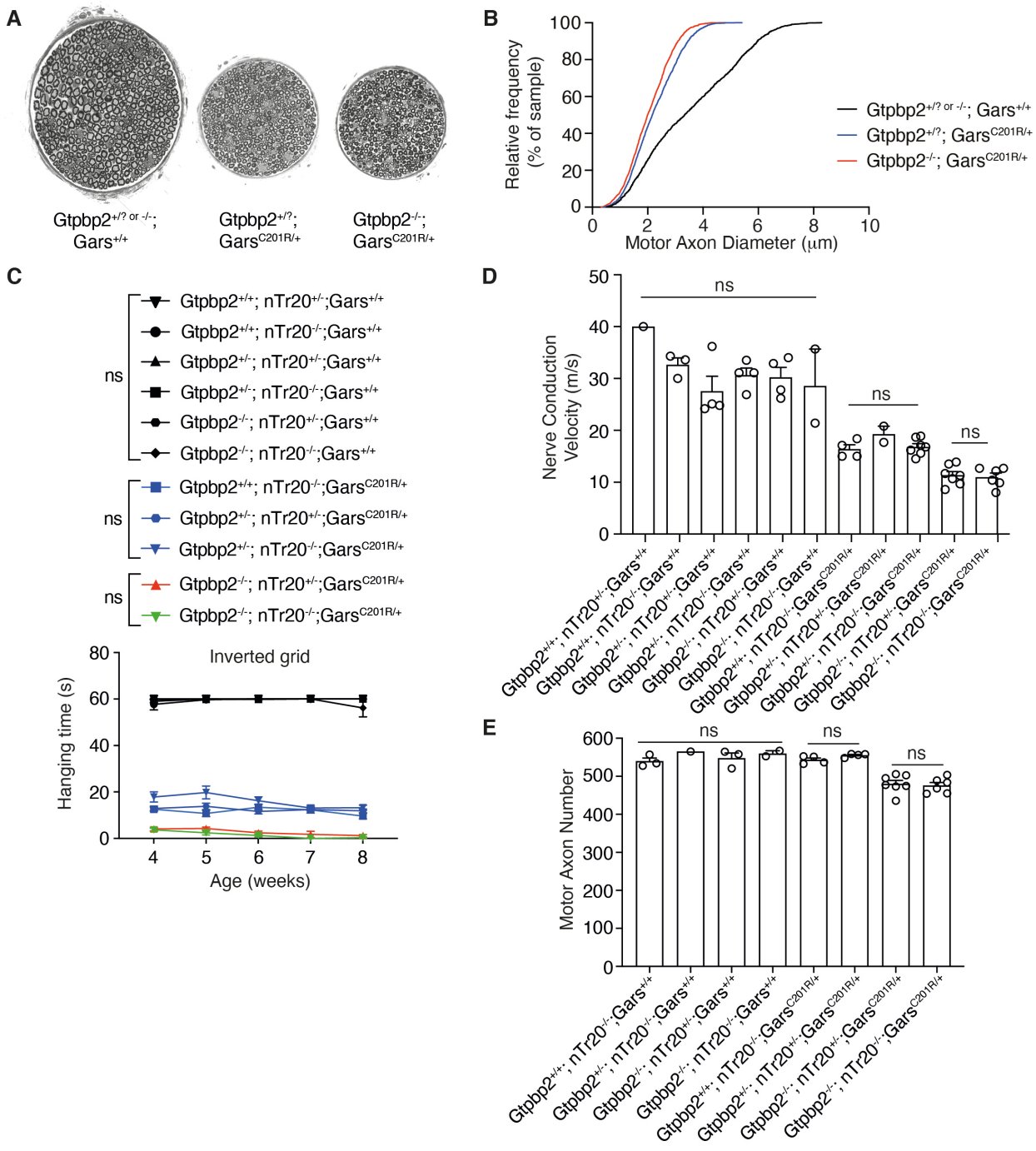

Fig. S14. Loss of *Gtpbp2* function aggravates peripheral neuropathy phenotypes in *Gars*$^{C201R/+}$ mice.

(**A**) Representative images of semi-thin sections through the motor branch of the femoral nerve of *Gtpbp2*$^{+/? \text{ or } -/-}$; *Gars*$^{+/+}$ (control), *Gtpbp2*$^{+/?}$; *Gars*$^{C201R/+}$, and *Gtpbp2*$^{-/-}$; *Gars*$^{C201R/+}$ littermate mice at 8 weeks of age. (**B**) Cumulative frequency of axon diameters in the motor branch of the femoral nerve of *Gtpbp2*$^{+/? \text{ or } -/-}$; *Gars*$^{+/+}$, *Gtpbp2*$^{+/?}$; *Gars*$^{C201R/+}$, and *Gtpbp2*$^{-/-}$; *Gars*$^{C201R/+}$ littermate mice at 8 weeks of age. n=3-4 per genotype group; ***p<0.001 for all comparisons between genotypes by Kolmogorov-Smirnov test. (**C**) Hanging time in the inverted grid test of

male mice of the indicated genotypes at 4, 5, 6, 7 and 8 weeks of age. n=4-10 mice per genotype. These data show that the genotypes that were pooled in Fig. 3E do not significantly differ from each other, as determined by one-way ANOVA. *Note*: nTr20 is one of the five $tRNA^{Arg\text{-}UCU}$-encoding genes, widely expressed in neurons and of the five $tRNA^{Arg\text{-}UCU}$ genes the one that is most highly expressed in the brain. The nTr20 mutation depletes the $tRNA^{Arg\text{-}UCU}$ pool and causes ribosome stalling. In combination with loss of Gtpbp2 function, this mutation causes neurodegeneration (*20*). (**D**) Nerve conduction velocity of the sciatic nerve of mice of the indicated genotypes at 8 weeks of age. n=1-6 mice per genotype. These data show that the genotypes that were pooled in Fig. 3F do not significantly differ from each other, as determined by one-way ANOVA. (**E**) Axon number in the motor branch of the femoral nerve of mice of the indicated genotypes at 8 weeks of age. n=1-6 per genotype. These data show that the genotypes that were pooled in Fig. 3G do not significantly differ from each other, as determined by one-way ANOVA. Graphs represent mean ± SEM.

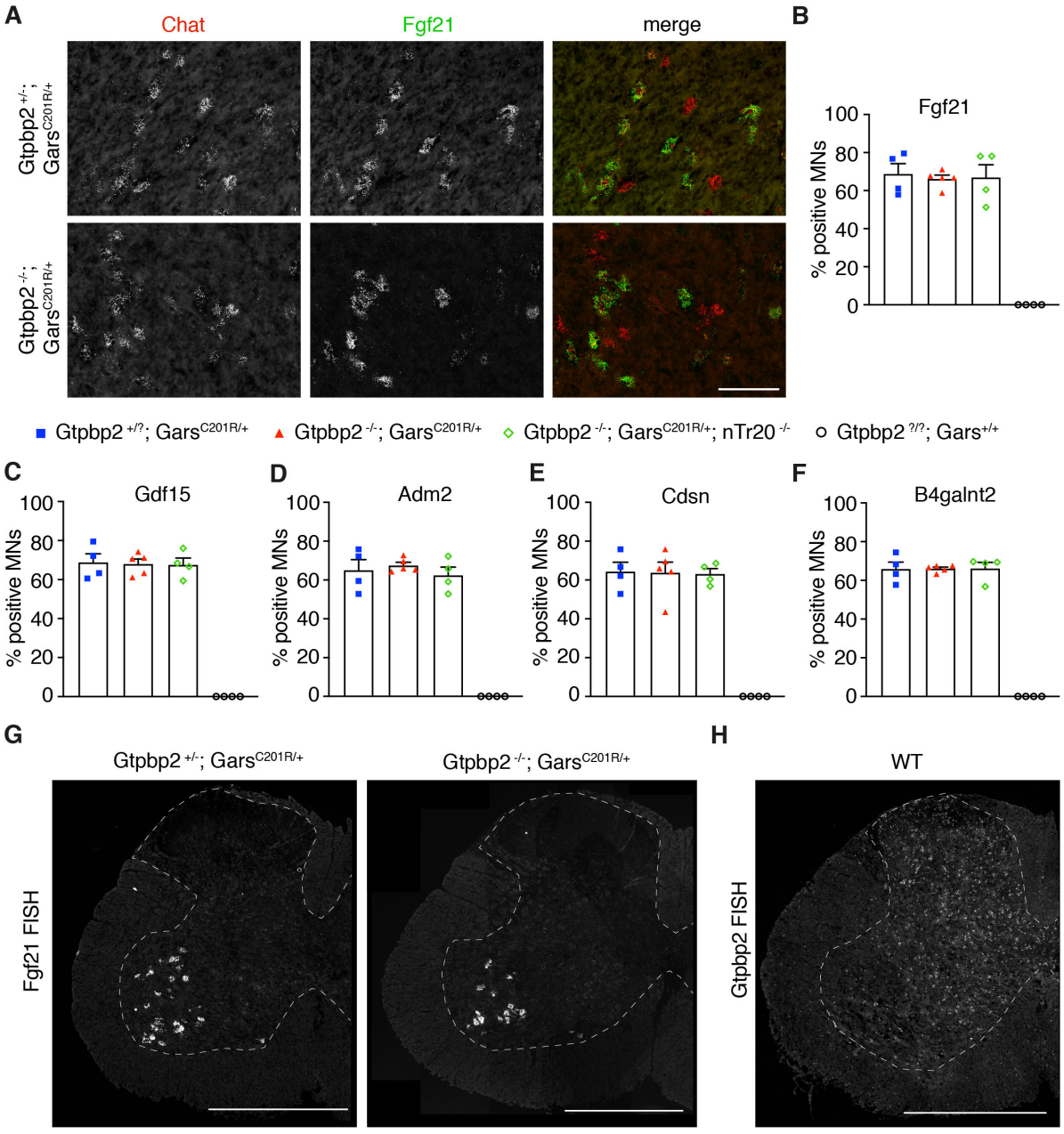

Fig. S15. ISR activation remains restricted to alpha motor neurons in *Gtpbp2$^{-/-}$; Gars$^{C201R/+}$* mice.

(**A**) Representative images of fluorescent in situ hybridization for *Chat* and *Fgf21* on spinal cord sections of *Gtpbp2$^{+/-}$; Gars$^{C201R/+}$* and *Gtpbp2$^{-/-}$; Gars$^{C201R/+}$* mice. Note that *Fgf21*-positive cells are also Chat-positive. Scale bar: 100µm. (**B-F**) Percentage of Chat-positive motor neurons (MNs) that coexpressed the ATF4 target genes *Fgf21* (B), *Gdf15* (C), *Adm2* (D), *Cdsn* (E), and *B4galnt2* (F) as determined by fluorescent in situ hybridization on spinal cord sections of *Gtpbp2$^{+/?}$; Gars$^{C201R/+}$*, *Gtpbp2$^{-/-}$; Gars$^{C201R/+}$*, *Gtpbp2$^{-/-}$; Gars$^{C201R/+}$; n-Tr20$^{-/-}$*, and *Gtpbp2$^{?/?}$; Gars$^{+/+}$* mice. (**G**) Overview images of fluorescent in situ hybridization for *Fgf21* on spinal cord sections of *Gtpbp2$^{+/-}$; Gars$^{C201R/+}$* and *Gtpbp2$^{-/-}$; Gars$^{C201R/+}$* mice, showing selective expression of *Fgf21* in large alpha motor neurons in the ventral horn. (**H**) Overview image of fluorescent in

situ hybridization for *Gtpbp2* on a spinal cord section of a WT mouse, showing widespread *Gtpbp2* expression. Graphs represent mean ± SEM.

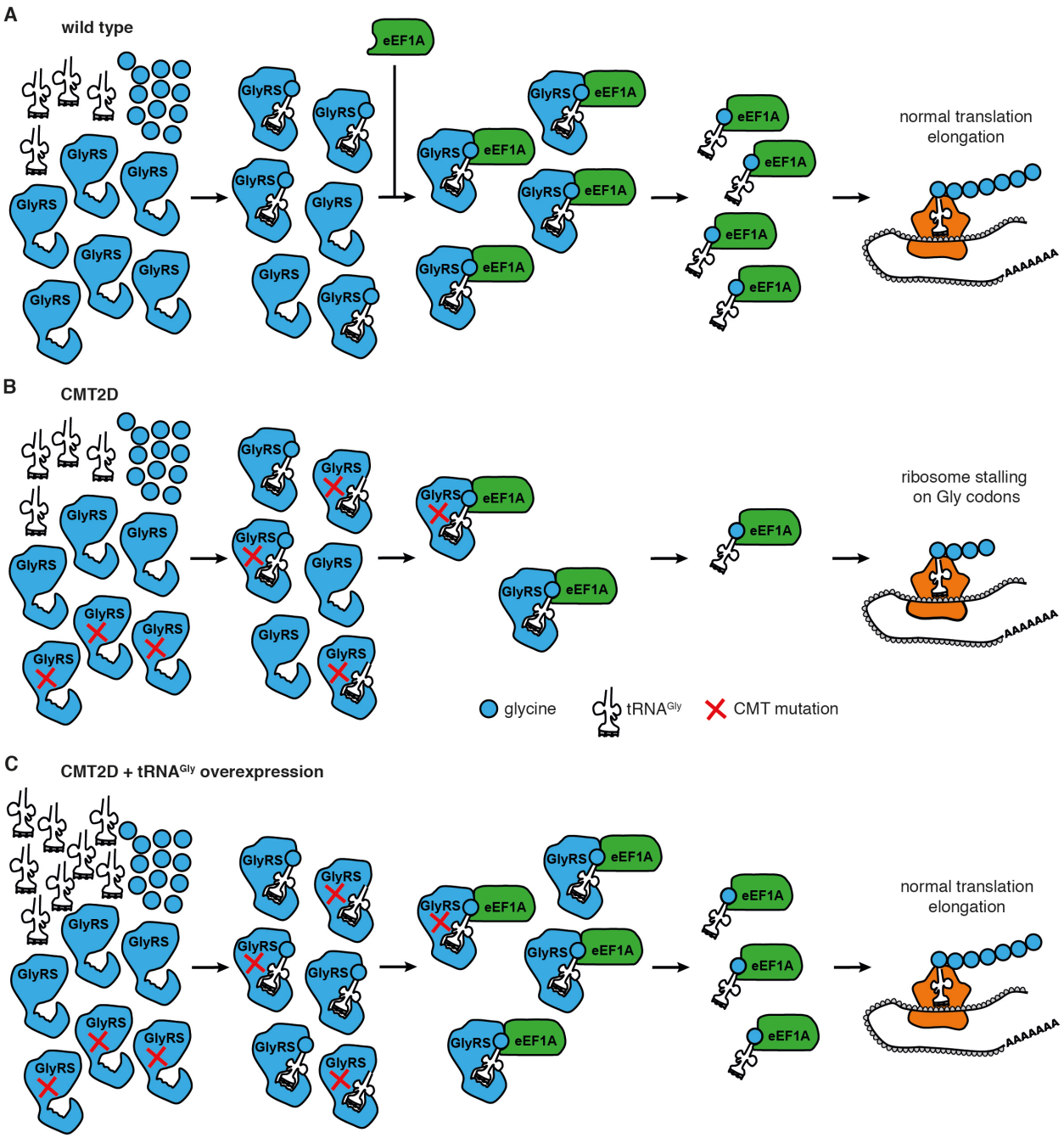

Fig. S16. Proposed molecular mechanism underlying CMT2D.

(**A**) WT GlyRS binds $tRNA^{Gly}$ and glycine, activates glycine, and aminoacylates $tRNA^{Gly}$ with glycine. Glycyl-$tRNA^{Gly}$ is transferred to eEF1A, which delivers glycyl-$tRNA^{Gly}$ to the ribosome for use in translation elongation. (**B**) In CMT2D, both WT and CMT-mutant (labeled with red cross) GlyRS proteins are present, derived from the WT and CMT-mutant *GARS* alleles, respectively. CMT-mutant GlyRS binds $tRNA^{Gly}$ and possibly glycine, may or may not activate glycine and aminoacylate $tRNA^{Gly}$, but fails to release $tRNA^{Gly}$ or releases it at a very slow pace. As a consequence, the cellular $tRNA^{Gly}$ pool is depleted below a critical threshold, leaving insufficient $tRNA^{Gly}$ for aminoacylation by WT GlyRS. This results in insufficient supply of

glycyl-tRNA^{Gly} to the ribosome, and stalling of the ribosome on Gly codons. (**C**) tRNA^{Gly} overexpression replenishes the cellular tRNA^{Gly} pool, resulting in sufficient tRNA^{Gly} for aminoacylation by WT GlyRS, sufficient glycyl-tRNA^{Gly} supply to the ribosome, and normal translation elongation.

5

GlyRS mutation	aminoacylation activity	protein synthesis	developmental lethality induced by motor neuron-selective expression	developmental lethality induced by ubiquitous expression	denervation of muscle 24	impaired climbing behavior	reduced dendritic coverage of MD sensory neurons	reduced life span
WT	=	=	-	-	-	-	-	-
E71G	=	↓↓	-	++	-	++	+	++
G240R	↓↓	↓↓↓	+++	+++	+++	+++	++	+++
G526R	↓↓↓	↓↓↓	++	+++	++	+++	++	+++

Table S1. Summary of peripheral neuropathy-like phenotypes in *Drosophila* CMT2D models.

As previously reported (*9*), UAS-transgenic lines were used for expression of WT or CMT-mutant (E71G, G240R, G526R) human GlyRS in *Drosophila*. The UAS-GAL4 system allows for spatial and temporal control over transgene expression (*54*). The three CMT-causing mutations were originally chosen because they segregated with disease in large multigenerational families (*55, 56*), and because of their differential effect on aminoacylation activity: GlyRS-E71G displays normal aminoacylation activity, while aminoacylation activity of GlyRS-G240R is severely reduced, and GlyRS-G526R displays full loss of aminoacylation activity (*7-9, 57*). The table shows the effect of expression of the different GlyRS transgenes on protein synthesis (evaluated by *in vivo* FUNCAT in motor and sensory neurons of third instar larvae (*9, 13*)), developmental lethality induced by motor neuron-selective (*OK371-GAL4*) or ubiquitous (*actin5C-GAL4*) expression, denervation of muscle 24 induced by motor neuron-selective (*OK371-GAL4*) expression in third instar larvae, impaired adult climbing behavior induced by motor neuron-selective (*OK371-GAL4*) expression as evaluated in the negative geotaxis assay, reduced dendritic coverage of class IV multidendritic (MD) sensory neurons upon selective expression in these neurons (*ppk-GAL4*), and reduced life span induced by ubiquitous expression from the adult stage onwards (*tub-GAL80^{ts}; tub-GAL4*). Symbols: = not altered; ↓ mild reduction; ↓↓ moderate reduction; ↓↓↓ severe reduction; - no phenotype; + mild phenotype; ++ moderate phenotype; +++ severe phenotype.

GlyRS fraction	GlyRS variant	K_{on} ($10^{-8}M^{-1}s^{-1}$)	K_{off} (s^{-1})
GlyRS dimer	WT	11 ± 6	13.4 ± 9.5 (100%)
	E71G	25 ± 2	13.3 ± 10.5 (92%)
	C157R	24 ± 3	21 (11%) to infinity (89%)
	G240R	27 ± 11	10 (4%) to infinity (96%)
	G526R	11 ± 5	14 (7%) to infinity (93%)
GlyRS monomer	C157R	>100	infinity (100%)
	G240R	>100	infinity (100%)
	G526R	>100	infinity (100%)

Table S2. K_{on} and K_{off} values of *Drosophila* tRNA$^{Gly\text{-}UCC}$ binding and release to the indicated human GlyRS variants.

K_{on} and K_{off} values are shown for the dimer and monomer fractions. The (percentage) in the K_{off} value column denotes the frequency of each measured value. Data are shown as mean ± SEM.

GlyRS mutation	**original amino acid**	**mutant amino acid**	**net effect**	**conservation**	**genetic evidence**	**ref**
A57V	hydrophobic	hydrophobic	no change	Chicken	single patient	(*58*)
E71G	negative	uncharged	+1 positive charge	Yeast	family	(*55*)
E71K	negative	positive	+2 positive charges	Yeast	single patient	(*59*)
L74R	hydrophobic	positive	+1 positive charge	Yeast	family	(*60*)
L129P	hydrophobic	uncharged	no change	Yeast	family	(*55*)
D146N	negative	uncharged	+1 positive charge	Yeast	family	(*61*)
D146Y	negative	hydrophobic	+1 positive charge	Yeast	single patient	(*62*)
C157R	uncharged	positive	+1 positive charge	*C. elegans*	mouse	(*15*)
D161H	negative	positive	+2 positive charges	*C. elegans*	family	(*63, 64*)
H162R	positive	positive	no change	Yeast	2 family members	(*59*)
S211F	uncharged	hydrophobic	no change	*C. elegans*	family	(*61*) (*65*)
L218Q	hydrophobic	uncharged	no change	Yeast	single patient	(*66*)
P234KY	uncharged	positive + hydrophobic	+1 positive charge	Yeast	mouse	(*31*)
M238R	hydrophobic	positive	+1 positive charge	Zebrafish	single patient	(*62*)
G240R	uncharged	positive	+1 positive charge	*Drosophila*	family	(*55*)
P244L	uncharged	hydrophobic	no change	Yeast	single patient	(*67*)
245-248 delETAQ	negative	/	+1 positive charge	*E. coli*	single patient, mouse	(*16*)
G273R	uncharged	positive	+1 positive charge	Yeast	single patient	(*59*)
E279D	negative	negative	no change	Yeast	family	(*68*)
I280F	hydrophobic	hydrophobic	no change	Yeast	single patient	(*69*)
H418R	positive	positive	no change	Yeast	family	(*70*)
K456Q	positive	negative	-2 positive charges	Yeast	2 family members	(*59*)
D500N	negative	uncharged	+1 positive charge	*Drosophila*	family	(*71*)
G526R	uncharged	positive	+1 positive charge	Yeast	family	(*55, 56*)
G598A	uncharged	hydrophobic	no change	*C. elegans*	single patients	(*69, 72*)

Table S3. Overview of CMT2D or distal hereditary motor neuropathy type V (dHMN-V) mutations, including their effect on GlyRS protein charge, evolutionary conservation of the affected amino acid residues, and genetic evidence to support disease causality.

Segregation of the mutation with CMT2D in a family provides stronger genetic evidence than mutations found in single patients. In mutant mouse lines, the causal link between the GlyRS mutation and peripheral neuropathy is established. The GlyRS mutations included in this study are in bold. Amino acid residues are numbered according to the cytoplasmic GlyRS isoform.

aaRS mutation	original amino acid	mutant amino acid	net effect	conservation	genetic evidence	ref
TyrRS G41R	uncharged	positive	+1 positive charge	*E. coli*	family	(*73*)
TyrRS D81I	negative	hydrophobic	+1 positive charge	Yeast	single patient	(*74*)
TyrRS 153-156 delVKQV	positive	/	-1 positive charge	Yeast	single patient	(*73*)
TyrRS E196K	negative	positive	+2 positive charge	Yeast	family	(*73*)
TyrRS E196Q	negative	uncharged	+1 positive charge	Yeast	family	(*75*)
AlaRS N71Y	uncharged	hydrophobic	no change	Yeast	single patient	(*76*)
AlaRS G102R	uncharged	positive	+1 positive charge	*E. coli*	family	(*77*)
AlaRS F175L	hydrophobic	hydrophobic	no change	*E. coli*	single patient	(*78*)
AlaRS R326W	positive	hydrophobic	-1 positive charge	*E. coli*	family	(*79*)
AlaRS R329H	positive	positive	no change	*E. coli*	family	(*80-82*)
AlaRS E337K	negative	positive	+2 positive charges	*Drosophila*	family	(*79*)
AlaRS S627L	uncharged	hydrophobic	no change	*E. coli*	family	(*79*)
AlaRS E688G	negative	uncharged	+1 positive charge	*E. coli*	family	(*82*)
AlaRS E778A	negative	hydrophobic	+1 positive charge	Rat	family	(*81*)
AlaRS D893N	negative	uncharged	+1 positive charge	*Drosophila*	family	(*83*)
HisRS T132I	uncharged	hydrophobic	no change	*E. coli*	family	(*84*)
HisRS V133F	hydrophobic	hydrophobic	no change	Yeast	single patient	(*85*)
HisRS P134H	uncharged	positive	+1 positive charge	Yeast	family	(*84*)
HisRS V155G	hydrophobic	uncharged	no change	Yeast	family	(*86*)
HisRS D175E	negative	negative	no change	Yeast	family	(*84*)
HisRS Y330C	hydrophobic	uncharged	no change	*E. coli*	family	(*86*)
HisRS D364Y	negative	hydrophobic	+1 positive charge	*E. coli*	family	(*84*)
TrpRS F138Y	hydrophobic	hydrophobic	no change	vertebrates	single patient	(*87*)
TrpRS H257R	positive	positive	no change	Zebrafish	family	(*88*)
TrpRS D314G	negative	uncharged	+1 positive charge	*Drosophila*	family	(*89*)
MetRS R618C	positive	uncharged	-1 positive charge	Yeast	single patients	(*90*)
MetRS R737W	positive	hydrophobic	-1 positive charge	Yeast	family	(*91*)
MetRS P800T	uncharged	hydrophobic	no change	*C. Elegans*	single patients	(*74, 92*)

Table S4. Overview of CMT or dHMN mutations in TyrRS, AlaRS, HisRS, TrpRS, and MetRS, including their effect on protein charge, evolutionary conservation of the affected amino acid residues, and genetic evidence to support disease causality.

Transgene	Cloning Primers	Primer sequence
Drosophila tRNA$^{Gly-GCC}$ scramble	pEntr_BB_FW	CATTATTTGCCATCCAGCTG
	pEntr_BB_REV	CAAAGGCGGTAATACGGTTATC
	tRNA:Gly-GCC-1-1_fr1_FW	TAACCGTATTACCGCCTTTGCGGCCGCTTAAGTTAG TAAAACACCCACAC
	tRNA:Gly-GCC-1-1_fr1_REV	GGAGACCTTGTATCTTGGGGAAATCTCTTTATG
	tRNA:Gly-GCC-1-2_fr1_FW	CCCCAAGATACAAGGTCTCCAGAGGTCAC
	tRNA:Gly-GCC-1-2_fr1_REV	TACTAACAGCGTGGACACTGACCAAAGC
	tRNA:Gly-GCC-1-3_fr1_FW	CAGTGTCCACGCTGTTAGTAGTTGCTGTTG
	tRNA:Gly-GCC-1-3_fr1_REV	CAGCTGGATGGCAAATAATGCATATGTCCGGATCC TACTAGGACATAGAAACAACAC
	tRNA:Gly-GCC-1-8_fr2_FW	TAACCGTATTACCGCCTTTGGATCCAACTCTGCTAC GAATTCCCG
	tRNA:Gly-GCC-1-8_fr2_REV	CTCATGTCGCGGCCAACATGGCGTATGATTAATAG
	tRNA:Gly-GCC-1-9_fr2_FW	CATGTTGGCCGCGACATGAGTATGGCATG
	tRNA:Gly-GCC-1-9_fr2_REV	GCTGTCGGTTGTGCACCGCTGAAAAGCTG
	tRNA:Gly-GCC-1-11_fr2_FW	AGCGGTGCACAACCGACAGCAAGAAGAAG
	tRNA:Gly-GCC-1-11_fr2_REV	CAGCTGGATGGCAAATAATGCATATGCCTGTAGGA ATGTGGATGTAG
	pEntr_BB_REV	CTAACTTAAGCATATGCTAGCGGCCGCAAAGGCGG TAATACGGTTATC
	tRNA:Gly-GCC-1-1_fr3_FW	ACCGCCTTTGCGGCCGCTAGCATATGCTTAAGTTAG TAAAACACCCACAC
	tRNA:Gly-GCC-1-2_fr3_REV	TAGCAGAGTTGTGGACACTGACCAAAGC
	tRNA:Gly-GCC-1-8_fr3_FW	CAGTGTCCACAACTCTGCTACGAATTCCCG
	tRNA:Gly-GCC-1-8_fr3_REV	ATCAACAAGGGGCCAACATGGCGTATGATTAATAG
	tRNA:Gly-GCC-1-13_fr3_FW	CATGTTGGCCCCTTGTTGATTTGTGTAAAAATTG
	tRNA:Gly-GCC-1-13_fr3_REV	CAGCTGGATGGCAAATAATGCTCGAGGTTGCACGT AATTGTCGAG
Drosophila tRNA$^{Gly-UCC}$	pEntr_FW	tctagaGGTCACTATCAGTCAAAATAAAAT
	pEntr_REV	ggtaccCAAAGGCGGTAATACGGTTATC
	CH322-79F21_fr1_FW	taaccgtattaccgcctttgggtaccGGAACGCCTTGTTATTTATG
	CH322-79F21_fr1_REV	gaaatgagaaCAACTCGGTTTTTGTTCATTG
	CH322-79F21_fr2_FW	aaccgagttgTTCTCATTTCGCTTGTCATC
	CH322-79F21_fr2_REV	ccagaaactgCAAAAGATACGGCCTCAG
	CH322-79F21_fr3_FW	gtatcttttgCAGTTTCTGGGCGAGTTC
	CH322-79F21_fr3_REV	tattttgactgatagtgacctctagaGCCAACTAAGTCAAAAGCTG
mouse tRNA$^{Gly-GCC}$	Gly_GCC_FW	GTCTCAGGGATGACTGGGAGGG
	Gly_GCC_REV	GCTACTTCTGCTGTCTGGGCTCC
	Sequencing Primers	**Primer sequence**
Drosophila tRNA$^{Gly-GCC}$ scramble	pJet1.2_seq_FW	CGACTCACTATAGGGAGAGCGGC
	pJet1.2_seq_REV	AAGAACATCGATTTTCCATGGCAG
Drosophila tRNA$^{Gly-UCC}$	pEntr_seq_FW	CCTTTTTACGGTTCCTGGCC
	pEntr_seq_REV	TGCCAGGAAACAGCTATGACC
	Gly-UCC_fr2-3_seq_FW	AACCGAGTTGTTCTCATTTCGC
	Gly-UCC_fr2-3_seq_REV	AAGCGAAATGAGAACAACTCGG
	Gly-UCC_fr3-4_seq_FW	AGGCCGTATCTTTTGCAGTTTC
	Gly-UCC_fr3-4_seq_REV	CCAGAAACTGCAAAAGATACGGC
mouse tRNA$^{Gly-GCC}$	Gly_GCC_seq_FW	CTTGTTTGGTTGAGGGACCAGG
	Gly_GCC_seq_Rev	CAAACAGGACAAACCAGCCAGG

Table S5. Sequences of primers used for PCR and sequencing of the indicated transgenic constructs.

Species	probe target	probe sequence (5'➔3')
mouse	Mm_tRNA_Gly^{GCC}	GGCGAGAATTCTACCACTGAACCACCAA
mouse	Mm_tRNA_Val^{CAC}	AGGCGAACGTGATAACCACTACACTACGGA
Drosophila	Dm_tRNA_Gly^{GCC}	TGCATCGGCCGGGAATCGAA
Drosophila	Dm_tRNA_Gly^{UCC}	TAACCATTACACCACCGACGC
Drosophila	Dm_tRNA_Ala^{AGC}	TGGTGGAGATGCGGGGTATCGA

Table S6. Sequence and tRNA target of probes used for northern blotting.

mouse line	oligo	sequence
Gars^{C201R}	Gars_fw	TCACGTGCTTGCTCTAGCAAGAC
	Gars_rev	GCTGATGATGGAATCCAGGACTC
NMF205	NMF205_WT_fw	CAGTGCCAACACTGGAATCGAT
	NMF205_WT_rev	GGTCTTAGCACACAGGTCCA
	NMF205_MUT_fw	CAGTGCCAACACTGGAATCGTC
	NMF205_MUT_rev	GGTCTTAGCACACAGGTCCA
B6J	B6J_fw	GGACTTCTAATCCAGAGGTTGT
	B6J_rev	TATCCCATCACGAAGCAAAAC
B6N	B6N_fw	GGACTTCTAATCCAGAGGTTGC
	B6N_rev	TATCCCATCACGAAGCAAAAC
tRNA^{Gly}	tRNA-gly-GCC-5'_FW	GCCAGTGTGCTGGAATTCG
	tRNA-gly-GCC-5'_REV	GGCCAATGCAGTAGCAATCC
	tRNA-gly-GCC-3'_FW	CCAGTCTCCTGGACAGAGATAGC
	tRNA-gly-GCC-3'_REV	AATTCGCCCTTGCTACTTCTG
	CD79b_FW	GAGACTCTGGCTACTCATCC
	CD79b_REV	CCTTCAGCAAGAGCTGGGGAC

Table S7. Sequences of primers used for mouse genotyping.

target	oligo	sequence
$tRNA^{Gly\text{-}high/low}$ transgene	tRNAGly383_CN_fw	CTTTCAGGTGGAGATGAGGAAG
	tRNAGly383_CN_rev	CAGCCCAAGGACTACAGATTT
	tRNAGly383_CN_pr	AGAGTTCATAGGGAGTTGCTGGGC
$tRNA^{Gly\text{-}high}$ transgene	TLA_fw_1	TGAGCAGAAATCTGTAGTCC
	TLA_rev_1	GCTCTCTTTCCTGTCTCAAA
	TLA_fw_2	AGCCCTTGAGTCATCTGTAA
	TLA_rev_2	GGTCAGTTTCCTCACAGAAC
Gars mRNA	Gars_fw	GTGAACAAGACGCCCCACAC
	Gars_rev	CCCAGGTAATGTTGCCGTTG
Gdf15 mRNA	Gdf15_fw	ATGCCAACCAGAGCCGAGAG
	Gdf15_rev	GGGAGACCCTGACTCAGCG
Fgf21 mRNA	Fgf21_fw	CGCAGTCCAGAAAGTCTCCTG
	Fgf21_rev	ACATTGTAACCGTCCTCCAGC
B4galnt2 mRNA	B4galnt2_fw	AAACCGAACTGGATGTGGTGG
	B4galnt2_rev	TCCGTGTGAGCCAAGAAGAAG
Beta actin mRNA	b-Actin_fw	GATCTGGCACCACACCTTCT
	b-Actin_rev	GGGGTGTTGAAGGTCTCAAA

Table S8. Sequences of primers and probes used for copy number and TLA analysis in $tRNA^{Gly}$ transgenic mice and primers for quantitative real-time PCR (qPCR) to evaluate transcript levels of *Gars* and ATF4 target genes.

5